iScience

CellPress

Article

Perovskite Photovoltaic Modules: Life Cycle Assessment of Pre-industrial Production Process

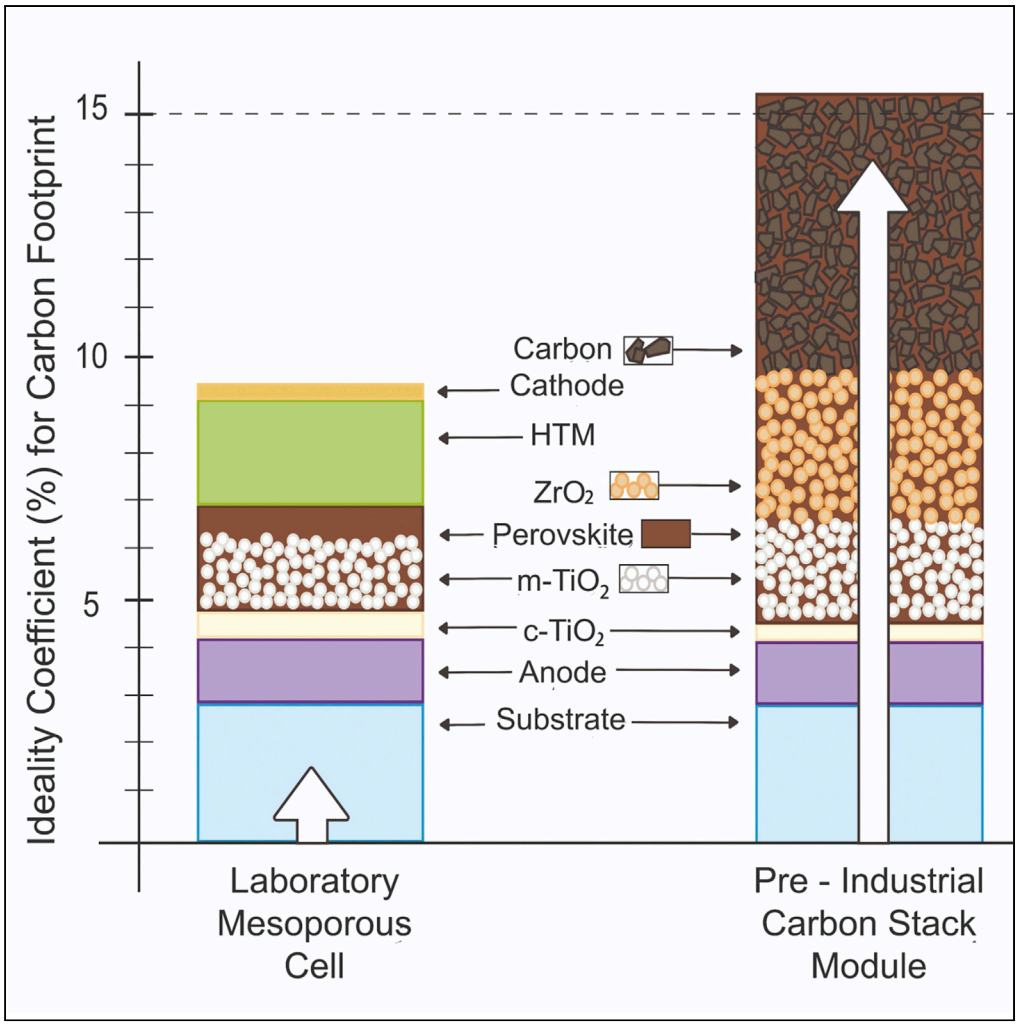

Jaume-Adrià Alberola-Borràs, Jenny A. Baker, Francesca De Rossi, ..., Katherine E.A. Hooper, Trystan M. Watson, Iván Mora-Seró

vidal@uji.es (R.V.)
sero@uji.es (I.M.-S.)

HIGHLIGHTS

LCA of a pre-industrial process of a carbon stack perovskite module

Laboratory, pre-industrial, and extrapolated ideal scenarios are compared

The pre-industrial process shows a significant improvement in environmental impact

Energy consumption is the main cause of the environmental impacts, not the Pb

Alberola-Borràs et al., iScience 9, 542–551
November 30, 2018
https://doi.org/10.1016/j.isci.2018.10.020

iScience

CellPress

Article

Perovskite Photovoltaic Modules: Life Cycle Assessment of Pre-industrial Production Process

Jaume-Adrià Alberola-Borràs,[1,3] Jenny A. Baker,[3,4] Francesca De Rossi,[3,4] Rosario Vidal,[1,*] David Beynon,[3,5] Katherine E.A. Hooper,[3,5] Trystan M. Watson,[3] and Iván Mora-Seró[2,6,*]

SUMMARY

Photovoltaic devices based on perovskite materials have a great potential to become an exceptional source of energy while preserving the environment. However, to enter the global market, they require further development to achieve the necessary performance requirements. The environmental performance of a pre-industrial process of production of a large-area carbon stack perovskite module is analyzed in this work through life cycle assessment (LCA). From the pre-industrial process an ideal process is simulated to establish a benchmark for pre-industrial and laboratory-scale processes. Perovskite is shown to be the most harmful layer of the carbon stack module because of the energy consumed in the preparation and annealing of the precursor solution, and not because of its Pb content. This work stresses the necessity of decreasing energy consumption during module preparation as the most effective way to reduce environmental impacts of perovskite solar cells.

INTRODUCTION

Photovoltaics (PV) represent a potential technology to mitigate the climate change and other pollution consequences while obtaining energy to power human activity (Chu et al., 2017). Nowadays, PV technologies based on halide perovskites have chiefly been developed at the laboratory scale, where it has raised much interest among the scientific community (Assadi et al., 2018). Its development is addressed in multiple ways: decreasing costs of production, enhancing its poor lifespan, guaranteeing safety despite its lead content or substituting it for another less toxic element, and producing them at industrial scale while maintaining high power conversion efficiency (PCE) (Chen et al., 2015; Fang et al., 2016; Zhang et al., 2016a). Thus far, there has been a fast progression in efficiencies that over 20% efficient perovskite solar cells (PSC) have been obtained in several laboratories around the world (Bi et al., 2016; Saliba et al., 2018, 2016; Shin et al., 2017; Tan et al., 2017; Yang et al., 2017). Nevertheless, for bringing PSCs to commercialization and launching them into the global market, as several companies aim to do (Edis, 2015; Gifford, 2015; Peleg, 2015; Sherahilo, 2018), paramount parameters encompass low cost, large area, high throughput, high solar-to-energy PCE, reproducibility, cost performance, long lifetime, and low environmental impact (Qiu et al., 2018).

The mainstream architecture and deposition techniques used in laboratories cannot be easily translated to larger substrates. For example, spin-coating or anti-solvent deposition methods present a large waste of material and a difficult implementation in large scale (Baker et al., 2017b; Jiang et al., 2018), besides leading to an increase of environmental impacts (Alberola-Borràs et al., 2018b). On the other hand, some materials used in several laboratory configurations such as spiro-MeOTAD or Au should be avoided for their high cost, reduced stability, and high environmental burden (Alberola-Borràs et al., 2018a; Meroni et al., 2018). Consequently, new architectures have been investigated to overcome these limitations. Architectures in which the perovskite is deposited through slot die (Burkitt et al., 2018; Cotella et al., 2017; Schmidt et al., 2015), blade coating (Baker et al., 2017b; Di Giacomo et al., 2015; Matteocci et al., 2014), and solvent-free pressure processing (Chen et al., 2017) are discarded because they still need an evaporated metal contact to complete the device or have low efficiencies (<5%). At the same time, a laminated device with a metal grid poly(3,4-ethylenedioxythiophene)polystyrene (PEDOT:PSS) cathode has been reported with an efficiency over 10% (Bryant et al., 2014a; Di Giacomo et al., 2015; Hooper et al., 2015), but the lifetime of this has not yet been proven. On the other hand, a large-area module based on a fully printed mesoporous stack, using carbon as cathode, has been reported, exhibiting low cost, high throughput, and high

[1]Grupo de Ingeniería de Diseño (GID), Departament d'enginyeria mecànica i construcció, Universitat Jaume I, Av. Sos Baynat s/n, 12071 Castelló, Spain

[2]Institute of Advanced Materials (INAM), Universitat Jaume I, Av. Sos Baynat, s/n, 12071 Castelló, Spain

[3]SPECIFIC, Swansea University, Bay Campus, Fabian Way, Swansea SA1 8EN, Wales, UK

[4]These authors contributed equally

[5]These authors contributed equally

[6]Lead Contact

*Correspondence: vidal@uji.es (R.V.), sero@uji.es (I.M.-S.)

https://doi.org/10.1016/j.isci.2018.10.020

stability (Baker et al., 2017a; Cai et al., 2017; Mei et al., 2014). In this configuration, the use of the expensive and unstable Spiro-MeOTAD and gold are avoided. As such, it is viewed as one of the closest to commercialization (Cai et al., 2017; Moulder et al., 1992). Perovskite is infiltrated into a semiconducting scaffold of mesoporous titania (m-TiO_2), an insulating scaffold of mesoporous zirconia (m-ZrO_2), and a cathode of carbon, whose porosity is crucial to control crystallization of the perovskite over a large area (Cotella et al., 2017). These layers are deposited through screen printing, which enables reproducibility in large-area substrates (Philip et al., 2016; Yasin et al., 2016). Despite the fact that infiltration of the precursor solution is usually conducted manually, recently an automated system to deposit the perovskite with a robotic dispenser and a mesh has demonstrated more homogeneous depositions on large areas (Meroni et al., 2018) and modules with active areas of up to 198 cm^2 have been reported (De Rossi et al., 2018). Furthermore, this configuration with a proper encapsulation exhibits outstanding lifetimes beyond 1 year (Grancini et al., 2017). By using different perovskite compositions in this carbon stack an efficiency close to 16% has been reached (Zhang et al., 2017c). Yet, tuning the perovskite composition with formamidinium, cesium, methylammonium, iodide, and bromide ions has led to adverse environmental consequences due to an increased amount of reagents (Alberola-Borràs et al., 2018b). Another advantage of the process is the usage of an ultra-fast annealing process with near-infrared radiation technique (Hooper et al., 2014). However, fluorine-doped tin oxide (FTO) remains the most expensive material in the structure (Park et al., 2016).

In addition to efficiency and cost issues, the environmental impact of the devices should be considered in the future implementation of this technology. The toxicity of lead embedded in perovskite remains one of the main concerns of PSCs since their early days (Park et al., 2016; Qiu et al., 2018; Rajagopal et al., 2018). Pb is notorious for its detrimental effects in the human body (Fewtrell et al., 2003; Qiu et al., 2018). Its damaging activity consists in the mimicry of the essential ions Ca, Zn, and Fe involved in biological processes (Babayigit et al., 2016b; Klaassen, 1980). Nonetheless, different studies have assured that its presence in PSCs should not pose a restrictive concern for its commercialization (Hailegnaw et al., 2015; Hauck et al., 2017). In fact, emissions of Pb stemming from other established applications are higher than those related to PSCs, such as lead-acid batteries, crystalline solar cell panels (during its production), and weather-proofing lead sheets on roofs (Gottesfeld and Pokhrel, 2011; Hauck et al., 2017). Still, PSCs embedded in consumer electronics or portable systems may find a barrier in the European market through the "RoHS Directive" (European Parliament, 2011), as it restricts the use of lead to 0.1% for homogeneous materials (Kadro and Hagfeldt, 2017). Several solutions to mitigate the detrimental effect of lead in PSCs have been proposed by the scientific community, such as designing safe production processes to prevent harmful consequences due to handling of Pb (Hauck et al., 2017) and efficient recycling processes for Pb as well as for the rest of the materials present in the solar cell (Chen et al., 2014; Kadro and Hagfeldt, 2017; Rajagopal et al., 2018; Zhang et al., 2016b). In parallel, Pb-free PSCs are under development using either Sn or Bi as substitutes (Abate, 2017; Jain et al., 2018; Liu et al., 2017), but their efficiencies are still quite low, and benefits in the environment, derived from the usage of these elements instead of Pb, are in doubt (Babayigit et al., 2016a; Serrano-Lujan et al., 2015).

A significant number of studies based on life cycle assessment (LCA) have been conducted to support PSCs on its way to commercialization. Some previous LCA studies, oriented toward the commercialization of perovskite PV modules, evaluated some techniques suitable for low-cost manufacturing. For instance, an LCA analyzing from cradle to gate two perovskite devices using spray and co-evaporation methods was reported (Celik et al., 2016). In contrast, the first LCA applied to PSCs compared two deposition methods, spin-coating and evaporation (Espinosa et al., 2015). Other LCAs likewise analyze laboratory-scale devices to find weak points and possible improvements from an early stage of PSC development (Alberola-Borràs et al., 2018a; Gong et al., 2015; Zhang et al., 2017a). Another LCA contrasting different configurations of Si/perovskite tandems concludes that the best configuration was free of spiro-MeOTAD and used Al instead of noble metals (Monteiro Lunardi et al., 2017). More analyses based on LCA contrast a handful of configurations of tandems with perovskite (Celik et al., 2017a, 2017b; Hauck et al., 2017; Itten and Stucki, 2017). LCA has been directly applied to the perovskite layer to contrast various compositions combining different cations and anions (Alberola-Borràs et al., 2018b). Similarly, different PSCs containing different perovskite compositions are compared in two studies (Ibn-Mohammed et al., 2017; Zhang et al., 2017b). The substitution of Pb for Sn in the perovskite layer is also analyzed in several studies (Babayigit et al., 2016a; Celik et al., 2017b; Serrano-Lujan et al., 2015). To the best of our knowledge, an LCA study directly applied to an industrial process of production of large-area PV modules based on perovskite has not been performed to date.

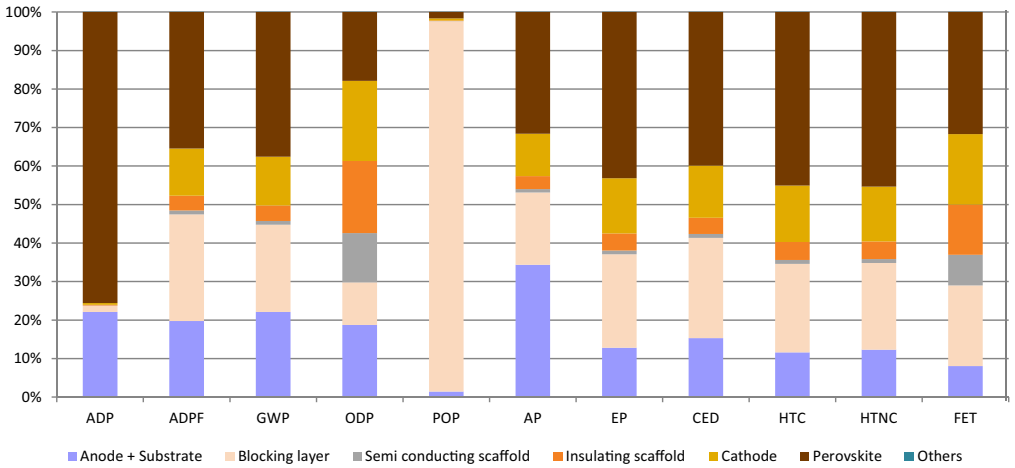

Figure 1. Aggregated Impacts of Each Layer of the Carbon Stack Perovskite Module, Sorted by Impact Categories

In this work, the environmental performance of a perovskite module, based on the carbon mesoporous stack architecture and produced with a pre-industrial process, is analyzed via LCA, from cradle to gate, to determine the major environmental impacts of each manufacturing step. This pre-industrial process is intended to be a preliminary step toward commercialization of perovskite modules. Remarkably, the energy consumptions of all equipment were directly measured and turned out to cause the most significant portion of environmental impact. The investigated process is based on a high-throughput process of production of a large-area module (hereafter referred to as pre-industrial module), reported in a previous work (De Rossi et al., 2018), to which some alterations are implemented (Baker et al., 2017a). Usage of data stemming from a pre-industrial process provides a good approach of the environmental impact that will generate a real process. In addition, an ideal industrial process of production, based on the pre-industrial one (hereafter referred to as the ideal module), is simulated (not directly measured) and environmentally assessed. In the ideal industrial process, energy consumption of some steps and usage of some materials are optimized with respect to those in the pre-industrial process, as it should be expected for the ideal implementation of a production line. We define an ideality coefficient that quantifies how close a given fabrication procedure is to the ideal process, in terms of environmental impacts. Finally, the progress attained by the large module produced via this pre-industrial process with respect to a small PSC produced by means of the most extended laboratory-scale process pertaining to a previous phase of development (hereafter referred to as laboratory-scale PSC) is illustrated via comparison of its ideality coefficient (Alberola-Borràs et al., 2018a).

RESULTS AND DISCUSSION

LCA of Pre-industrial Module

Environment wise, the production of a perovskite PV module with a carbon stack architecture (pre-industrial module) is scrutinized to elucidate its main weaknesses. For this purpose, the impact of each of the layers of the module is estimated for all the categories considered for this study, which is shown in Figure 1. Impacts of each layer are divided by the overall impact of the module. To make them comparable, impacts of each layer are aggregated per category. More information about how the environmental impacts are obtained can be found in Transparent Methods, and Tables S1 and S4–S9 in the Supplemental Information.

Distribution of impacts in Figure 1 exposes that the perovskite layer presents the biggest impact among all layers. Its contribution is superior to that of the rest of the layers, except in photochemical oxidation (POP) category. For most of the categories, the contribution of the perovskite layer is superior to 50%. In contrast, for ozone layer depletion (ODP), POP, and acidification (AP) categories, the impact of perovskite layer is below 50%. Most of the impact of the perovskite layer stems from the use of energy flow, except for the abiotic depletion (ADP) category where it mostly stems from the materials flow. Both heating up and annealing processes involved in the perovskite deposition contribute similarly to the impact. Both high

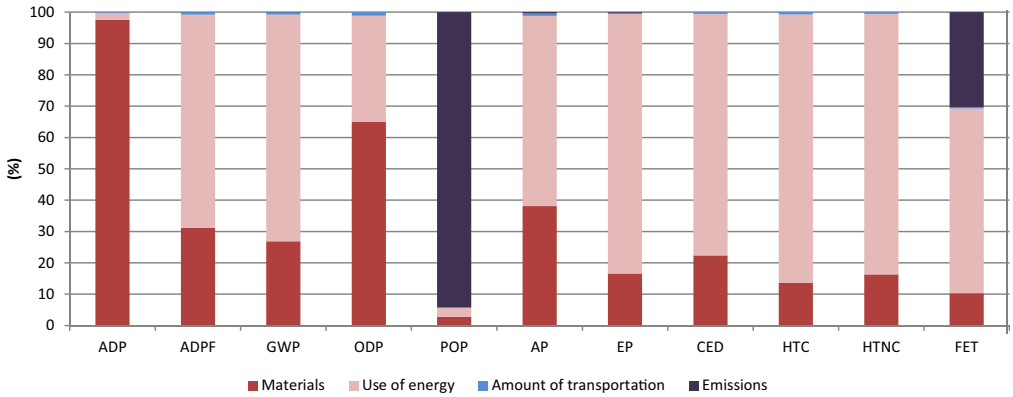

Figure 2. Aggregated Impacts of the Carbon Stack Perovskite Module, Sorted by Impact Categories

consumptions originate from a forced convection generated to assist perovskite crystallization during the annealing process and a process of heating of perovskite reagents carried out in a hot plate, which needs optimization. Thus, a reduction of its impact should be among the next goals to improve the sustainability of the pre-industrial process. For instance, the amount of precursor reagents could be reduced with an automatic deposition using a robot and a mesh, instead of depositing it manually (Meroni et al., 2018). A reduction of the energy required for heating up the precursor solution at 70°C and annealing the perovskite layer—e.g., via heat recovery and other methods for reducing the crystallization time—would also be necessary.

For the POP category, the most adverse layer is the blocking layer, accounting for more than 90% of the total. For this category, the impact mostly stems from the emissions. The most harmful compound emitted is isopropanol. The impact of blocking layer is also significant for the rest of the categories alongside the anode + substrate layer, whose contribution is above 10% in most of them. Use of energy and materials are the main responsible flows of their impact. Moreover, impact of the cathode is also noticeable.

To assist the analysis of the pre-industrial module, the distribution of impacts for each of the impact flow is depicted in Figure 2 for all categories. Materials, use of energy, amount of transportation, and emissions flows are included in this analysis. Impacts of each flow are divided by the total impact to obtain the percentage of contribution.

When the impact of the four types of flows are compared in Figure 2, the use of energy is seen to be the most detrimental for abiotic depletion (fossil fuel) (ADPF), climate change (GWP), AP, eutrophication (EP), cumulative energy demand (CED), human toxicity (cancer effects) (HTC), human toxicity (non-cancer effects) (HTNC), and freshwater ecotoxicity (FET) categories, varying between 69.1% and 90.2%. As well as it happens in Figure 3, impacts of those categories mainly stems from the perovskite layer, in particular from the heating up of the precursor solution and annealing of the film.

In contrast, for ADP and ODP the most harmful flow is materials, which ranges from 56.7% to 92.6%. For ADP category, lead iodide reagent for the perovskite production is the most harmful material: its impact is one order of magnitude higher than methylammonium iodide (MAI), two orders of magnitude higher than 5-ammonium valeric acid iodide (AVAI), and three orders of magnitude higher than the solvent γ-butyrolactone (GBL). Meanwhile, for ODP the main material responsible for the impact is not as clear, since all layers contribute roughly the same. For the POP category, the contribution of emissions flow is higher than 90%, due to the release of isopropanol used copiously as a carrier to enable the blocking layer deposition via spray.

As the materials chosen are an important concern for the production of PV devices and their impact is usually hidden by that of the use of energy flow, we focus on the materials used for the production of the pre-industrial module. The impact of each compound used is divided by the total impact of the materials flow and displayed in Figure 3, sorted by categories. As the impacts of some of the compounds depicted are too little to be appreciated in the chart, they are aggregated in a single group (others), which comprises

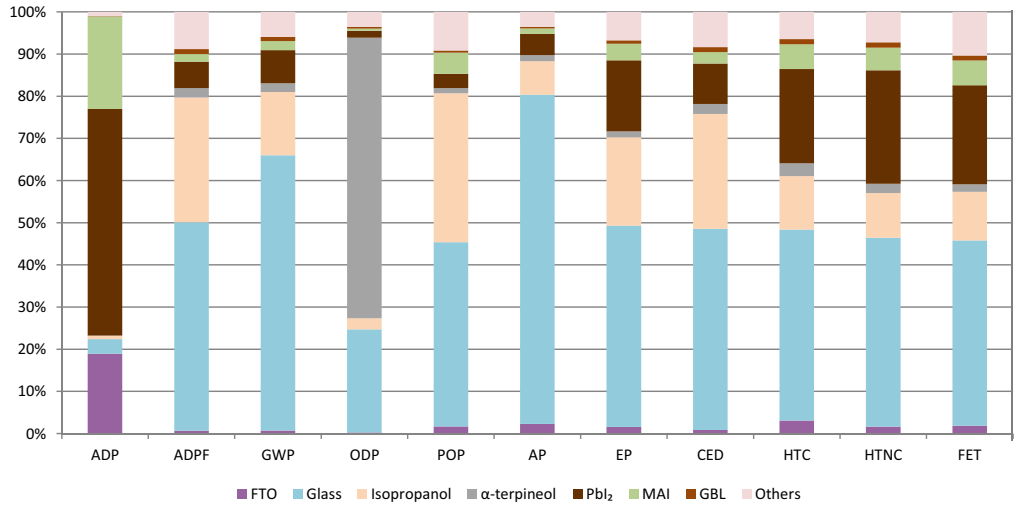

Figure 3. Aggregated Impacts of Material Inputs of the Carbon Stack Perovskite Module, Sorted by Impact Categories

TiAcAc, TiO_2, ethylcellulose, 2-(2-butoxyethoxy) ethyl acetate, nitrocellulose, AVAI, polyethylene terephthalate, zirconia, and carbon. On the other hand, contributions of the impact of FTO, glass substrate, isopropanol, α-terpineol, PbI_2, MAI, and GBL are shown individually.

The glass substrate, accounting for the largest fraction of the mass of the pre-industrial module, represents the most detrimental material. Its contribution is above 43% for all categories, except for ADP (slightly below 20%) and ODP. For the ADP category, the most harmful material, contributing nearly 60% to this category, is the PbI_2 used as reagent for the perovskite synthesis. The reason behind such contribution lies in the fact that a large amount of it is used and its impact per kilogram is high. Isopropanol and α-terpineol solvents have a significant contribution to the overall impact. Terpineol is especially detrimental for ODP category, where it represents nearly 67% of the total. On the other hand, mass of isopropanol used per kWh is the highest of all materials, i.e., 0.0908 kg/kWh. Impact of MAI is relatively modest except for ADP category, where it represents more than 20%. Moreover, GBL impacts are appreciable for every category. In consequence, the aggregate of compounds involved in the synthesis of perovskite (PbI_2, MAI, GBL) is higher than 10% for ADP, GWP, EP, CED HTC, HTNC, and FET. This fact reinforces the need for reducing the usage of reagents for the synthesis of perovskite as pointed out in the analysis in Figure 2.

Ideality Analysis

Minimization of material and energy consumption establishes the ideal scenario to decrease the environmental impacts caused by a device fabrication. Here, we define an ideality coefficient that quantifies how close a given fabrication procedure is to the ideal process, in percentage. Note that a technology requires an ideal coefficient as high as possible to reduce as much as possible the environmental impacts. However, no technological process can reach 100% ideality coefficient, as no technology can produce zero waste material and consume just the thermodynamic limit energy. This coefficient is depicted in percentages for both the pre-industrial module and the laboratory-scale PSC in Figure 4. Its value is the result of dividing the impact of the ideal process by the impact of the process to compare. For this analysis, the most fundamental categories are only used to ease its performance and thus its comprehension. As previously discussed and according to the data reported in Figure 1, the most concerning layers of the pre-industrial module are the anode + substrate, the blocking layer, and the perovskite, so these are the only layers included in the analysis. To assess in great detail these layers, this analysis is combined with the relative impacts—sorted by type of flow—of both the carbon stack module produced at pre-industrial scale and the PSC produced at the laboratory scale. The impact of each flow type pertaining to each layer is resized and aggregated to fit in the corresponding percentage of ideality coefficient. Results are sorted by device, by category, and finally by layer, where those of the anode + substrate layer (Figure 4A) are depicted from 0% to 100% and those of the blocking and perovskite layers (Figure 4B) are depicted from 0% to 1%. Further

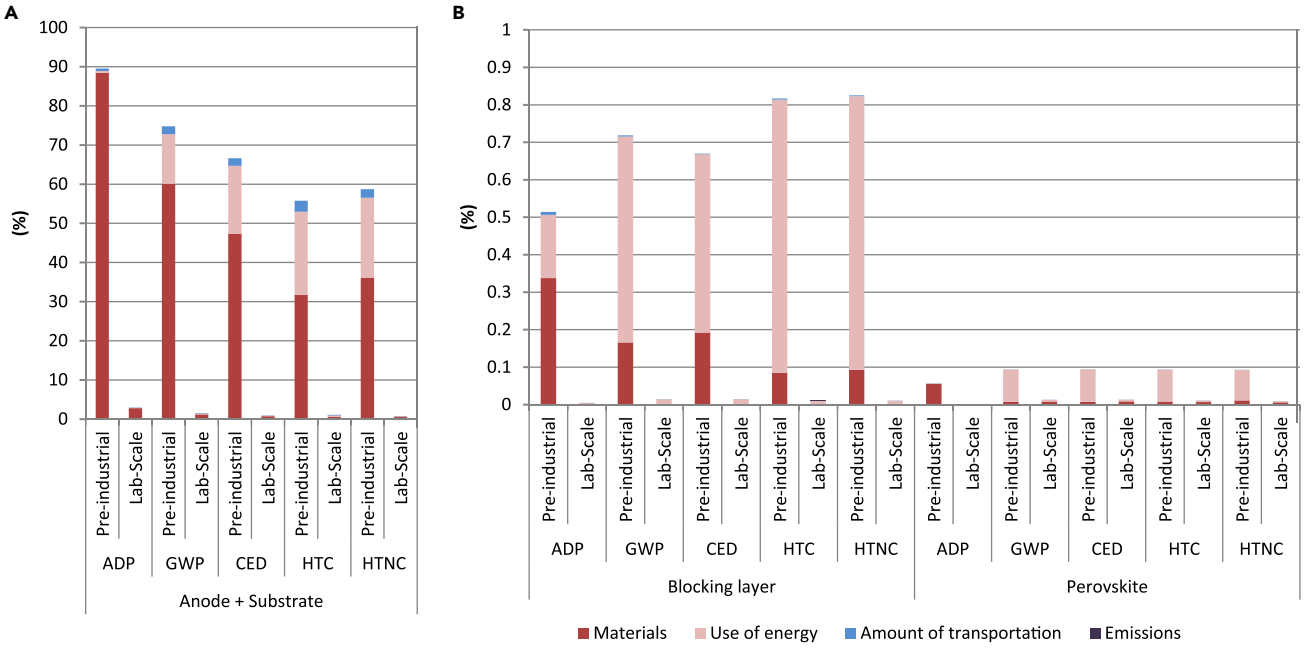

Figure 4. Ideality Coefficient for the Carbon Stack Module Produced with a Pre-industrial Process and the PSC Produced with a Process in the Laboratory Environment

The ideality coefficient quantifies how close a given fabrication procedure is to the ideal process, in percentage; its value is the result of dividing the impact of the ideal process by the impact of the process to compare. Relative impacts from pre-industrial module, PSC at laboratory scale, and ideal process, sorted by impact categories and layers: (A) anode + substrate, (B) blocking and perovskite layer.

See also Figures S1 and S2 in the Supplemental Information.

information about how these outcomes are obtained can be found in Tables S1–S9 and the Transparent Methods section in the Supplemental Information.

From the results in Figure 4, it is observed that the pre-industrial module reduces significantly all impacts, with ideality coefficients reaching values as high as 89.5% for ADP. In the anode + substrate layer, the pre-industrial process reaches the highest ideality coefficients among the three layers analyzed, where the pre-industrial device ranges from 55.8% to 89.5%. It is important to bear in mind that the cleaning step has been removed for the anode + substrate with respect to the process performed in the laboratory, which is the cause of the reduction in the impact of this layer. Remarkably, impacts derived from anode + substrate layer of both pre-industrial and ideal processes are almost alike, indicating that further optimization of the pre-industrial process should focus on the blocking layer and especially the perovskite layer. Theoretical optimization of materials and energy in the ideal process is the reason why ideality coefficient of the pre-industrial process is not closer to 100%. The materials flow is the most responsible for the impact of the anode + substrate, followed by the energy for all categories except ADP. The high values of the ideality coefficient of the pre-industrial process contrast with those of the laboratory-scale PSC, which does not surpass 3.0% (about 30-fold less), which reinforces the progression made by the pre-industrial process for the anode + substrate layer.

Ideality coefficients for the blocking layer are significantly lower, ranging from 0.51% to 0.83% for the pre-industrial process, where the highest ideality coefficient pertains to the HTNC category. However, it is far from the ideal process, mostly due to the use of energy flow for the blocking layer. For the blocking layer, a significant optimization of both materials and use of energy flows is recommended to improve ideality. For instance, depositing this layer by screen printing would result in the optimization of TiAcAc solution and a decrease in the usage of energy, as it happens for the mesoporous layers in the pre-industrial process. Furthermore, a reduction in the thickness of the blocking layer to 8 nm is feasible, via electrophoretic deposition method, with a subsequent reduction in materials (Li et al., 2015). Other deposition methods such as spray-cast and semi-automatic spray pyrolysis might pose an

alternative for the industrial manufacture of the carbon-stack perovskite module (Bishop et al., 2017; Krýsová et al., 2018). For the laboratory-scale process, ideality coefficients fluctuate between 0.0043% and 0.0143%, which are well below those of the pre-industrial one (about 58-fold less). Therefore, for the blocking layer the pre-industrial process is less harmful, which highlights the advancement it has achieved.

In addition, results reveal that the process of deposition of perovskite is the least optimized, narrowly followed by the blocking layer. Its ideality coefficients vary between 0.06% for the ADP category and 0.09% for GWP, CED, HTC, and HTNC categories. The highest amount of energy consumed for the pre-industrial process, to prepare the solution and to anneal the deposited layer, is responsible for these striking results because use of energy is the most detrimental flow for this layer. Therefore, finding an alternative, such as heating with near-infrared radiation (Baker et al., 2017a; Hooper et al., 2014), especially for the annealing step, should be fundamental to reduce the impact of this process to that of the ideal process and get it off the ground. Alternatively, using other heating techniques needing shorter operational times such as near-infrared radiation (Bryant et al., 2014b; Troughton et al., 2015), photonic flash-annealing (Troughton et al., 2016), and high-temperature, short-time annealing processes (Kim et al., 2017) could optimize the environmental performance of the perovskite layer. When compared with those of the laboratory-scale PSC, ideality coefficient values of the pre-industrial device are notably higher (about 8-fold higher), despite the fact that both processes are far from ideality, pointing out the improvement already achieved. The overall outcomes of the study are provided in Tables S10–S12 of the Supplemental Information.

Conclusions

A cradle-to-gate LCA of a pre-industrial process of production of a large-area perovskite module based on a carbon stack architecture is assessed. An ideality coefficient is obtained to evaluate the level of optimization of the pre-industrial module, which shows overall encouraging results. This ideality coefficient of the pre-industrial process is compared with that of a mesoporous structured PSC produced in the laboratory environment and with an extrapolated ideal situation in which material and energy consumption is minimized.

The perovskite layer is found to be the layer with the greatest impact on the pre-industrial module, mainly due to the energy consumed in the preparation and annealing of the precursor solution, rather than the Pb content, which raises a greater concern. This step is highly amenable to optimization.

Ideality coefficients of the pre-industrial process show a significant improvement regarding environmental impacts for the most relevant layers, namely, the FTO-glass substrate, the compact TiO_2 blocking layer, and the perovskite. The first one generates low impacts, and is already close to optimal, whereas the energy consumptions of the perovskite and blocking layers are still too high and must be reduced.

Limitation of the Study

This study presents the environmental impacts of a large-area perovskite PV module produced with a pre-industrial process, which are obtained by a LCA. Due to the novel state of development of this process, encapsulation and contacts of the resulting PV module are not definite to date. Therefore, they were not included in the system analyzed herein. In parallel, some other assumptions were taken, such as the substrate and the anode are deposited right before the module deposition, and thus there is no need of applying a cleaning process onto them. The stability and efficiency of the PV devices based on perovskite can be significantly improved in the near future. However, in this study, their current empirical values are utilized. The LCA is performed from cradle to gate, therefore usage and end-of-life phases are not included in this work. Finally, among all the existing processes to produce large-scale perovskite PV modules, this study tackles the closest process to commercialization.

METHODS

All methods can be found in the accompanying Transparent Methods supplemental file.

SUPPLEMENTAL INFORMATION

Supplemental Information includes Transparent Methods, 4 figures, 14 tables, and 1 data file and can be found with this article online at https://doi.org/10.1016/j.isci.2018.10.020.

ACKNOWLEDGMENTS

This work was partially supported by the European Research Council (ERC) via Consolidator Grant (724424 - No-LIMIT), the Engineering and Physical Sciences Research Council (EPSRC) through the SPECIFIC Innovation and Knowledge Center (EP/N02083/1) and Self assembly of Perovskite Absorber layers - Cells Engineered into Modules Project (EP/M01524/1), and the Fundación Balaguer-Gonel Hermanos. We greatly acknowledge Nuria Vernís for her contribution in the design of the figures of this manuscript.

AUTHOR CONTRIBUTIONS

J.-A.A.-B. modeled the reagents, collated the data, and executed the analysis. J.-A.A.-B. and R.V. wrote the first version of the manuscript. J.A.B. and F.D.R. collated data and supervised direct data measurements. D.B. and K.E.A.H. assisted the data collation. R.V., T.M.W., and I.M.-S. proposed and supervised the work. All authors revised and contributed to the final version of the manuscript.

DECLARATION OF INTERESTS

The authors declare no competing interests.

Received: July 18, 2018
Revised: October 5, 2018
Accepted: October 16, 2018
Published: November 14, 2018

REFERENCES

Abate, A. (2017). Perovskite solar cells go lead free. Joule *1*, 659–664.

Alberola-Borràs, J.-A., Vidal, R., Juárez-Pérez, E.J., Mas-Marzá, E., Guerrero, A., and Mora-Seró, I. (2018a). Relative impacts of methylammonium lead triiodide perovskite solar cells based on life cycle assessment. Sol. Energy Mater. Sol. Cells *179*, 169–177.

Alberola-Borràs, J.-A., Vidal, R., and Mora-Seró, I. (2018b). Evaluation of multiple cation/anion perovskite solar cells through life cycle assessment. Sustain. Energy Fuels *2*, 1600–1609.

Assadi, M.K., Bakhoda, S., Saidur, R., and Hanaei, H. (2018). Recent progress in perovskite solar cells. Renew. Sustain. Energy Rev. *81*, 2812–2822.

Babayigit, A., Duy Thanh, D., Ethirajan, A., Manca, J., Muller, M., Boyen, H.-G., and Conings, B. (2016a). Assessing the toxicity of Pb- and Sn-based perovskite solar cells in model organism *Danio rerio*. Sci. Rep. *6*, 18721.

Babayigit, A., Ethirajan, A., Muller, M., and Conings, B. (2016b). Toxicity of organometal halide perovskite solar cells. Nat. Mater. *15*, 247–251.

Baker, J., Hooper, K., Meroni, S., Pockett, A., McGettrick, J., Wei, Z., Escalante, R., Oskam, G., Carnie, M., and Watson, T. (2017a). High throughput fabrication of mesoporous carbon perovskite solar cells. J. Mater. Chem. A *5*, 18643–18650.

Baker, J.A., Mouhamad, Y., Hooper, K.E.A., Burkitt, D., Geoghegan, M., and Watson, T.M. (2017b). From spin coating to roll-to-roll: investigating the challenge of upscaling lead halide perovskite solar cells. IET Renew. Power Gener. *11*, 546–549.

Bi, D., Tress, W., Dar, M.I., Gao, P., Luo, J., Renevier, C., Schenk, K., Abate, A., Giordano, F., Correa Baena, J.-P., et al. (2016). Efficient luminescent solar cells based on tailored mixed-cation perovskites. Sci. Adv. *2*, e1501170.

Bishop, J.E., Mohamad, D.K., Wong-Stringer, M., Smith, A., and Lidzey, D.G. (2017). Spray-cast multilayer perovskite solar cells with an active-area of 1.5 cm2. Sci. Rep. *7*, 7962.

Bryant, D., Greenwood, P., Troughton, J., Wijdekop, M., Carnie, M., Davies, M., Wojciechowski, K., Snaith, H.J., Watson, T., and Worsley, D. (2014a). A transparent conductive adhesive laminate electrode for high-efficiency organic-inorganic lead halide perovskite solar cells. Adv. Mater. *26*, 7499–7504.

Bryant, D., Mabbett, I., Greenwood, P., Watson, T., Wijdekop, M., and Worsley, D. (2014b). Ultrafast near-infrared curing of PEDOT: PSS. Org. Electron. *15*, 1126–1130.

Burkitt, D., Searle, J., and Watson, T. (2018). Perovskite solar cells in N-I-P structure with four slot-die-coated layers. R. Soc. Open Sci. *5*, 172158.

Cai, M., Wu, Y., Chen, H., Yang, X., Qiang, Y., and Han, L. (2017). Cost-performance analysis of perovskite solar modules. Adv. Sci. *4*, 1600269.

Celik, I., Philips, A.B., Song, Z., Yan, Y., Ellingson, R.J., Heben, M.J., and Apul, D. (2017a). Energy payback time (EPBT) and energy return on energy invested (eroi) of perovskite tandem photovoltaic solar cells. IEEE J. Photovolt. *8*, 305–309.

Celik, I., Phillips, A.B., Song, Z., Yan, Y., Ellingson, R.J., Heben, M.J., and Apul, D. (2017b). Environmental analysis of perovskites and other relevant solar cell technologies in a tandem configuration. Energy Environ. Sci. *10*, 1874–1884.

Celik, I., Song, Z., Cimaroli, A.J., Yan, Y., Heben, M.J., and Apul, D. (2016). Life Cycle Assessment (LCA) of perovskite PV cells projected from lab to fab. Sol. Energy Mater. Sol. Cells *156*, 157–169.

Chen, H., Ye, F., Tang, W., He, J., Yin, M., Wang, Y., Xie, F., Bi, E., Yang, X., Grätzel, M., and Han, L. (2017). A solvent- and vacuum-free route to large-area perovskite films for efficient solar modules. Nature *550*, 92–95.

Chen, P.-Y., Qi, J., Klug, M.T., Dang, X., Hammond, P.T., and Belcher, A.M. (2014). Environmentally responsible fabrication of efficient perovskite solar cells from recycled car batteries. Energy Environ. Sci. *7*, 3659–3665.

Chen, Q., De Marco, N., Yang, Y., Song, T.-B., Chen, C.-C., Zhao, H., Hong, Z., Zhou, H., and Yang, Y. (2015). Under the spotlight: the organic–inorganic hybrid halide perovskite for optoelectronic applications. Nano Today *10*, 355–396.

Chu, S., Cui, Y., and Liu, N. (2017). The path towards sustainable energy. Nat. Mater. *16*, 16–22.

Cotella, G., Baker, J., Worsley, D., De Rossi, F., Pleydell-Pearce, C., Carnie, M., and Watson, T. (2017). One-step deposition by slot-die coating of mixed lead halide perovskite for photovoltaic applications. Sol. Energy Mater. Sol. Cells *159*, 362–369.

De Rossi, F., Baker, J.A., Beynon, D., Hooper, K.E.A., Meroni, S.M.P., Williams, D., Wei, Z., Yasin, A., Charbonneau, C., Jewell, E.H., and Watson, T.M. (2018). All printable perovskite solar modules with 198 cm^2 active area and over 6% efficiency. Adv. Mater. Technol. 1800156. https://doi.org/10.1002/admt.201800156.

Di Giacomo, F., Zardetto, V., D'Epifanio, A., Pescetelli, S., Matteocci, F., Razza, S., Di Carlo, A., Licoccia, S., Kessels, W.M.M., Creatore, M., and Brown, T.M. (2015). Flexible perovskite photovoltaic modules and solar cells based on

atomic layer deposited compact layers and UV-irradiated TiO 2 scaffolds on plastic substrates. Adv. Energy Mater. *5*, 1401808.

Edis, T., (2015). Dyesol awarded $0.5m grant to pursue high efficiency, low cost solar cell. Aust. (Last Accessed: 30/10/2018). https://www.theaustralian.com.au/business/business-spectator/dyesol-awarded-05m-grant-to-pursue-high-efficiency-low-cost-solar-cell/news-story/02bc43e776185abe903642bc8129c79b.

Espinosa, N., Serrano-Luján, L., Urbina, A., and Krebs, F.C. (2015). Solution and vapour deposited lead perovskite solar cells: Ecotoxicity from a life cycle assessment perspective. Sol. Energy Mater. Sol. Cells *137*, 303–310.

European Parliament. (2011). Directive 2011/65/EU of the European Parliament and of the Council of 8 June 2011, on the restriction of the use of certain hazardous substances in electrical and electronic equipment (RoHS). Off. J. Eur. Comm. *54*, 88–110.

Fang, R., Zhang, W., Zhang, S., and Chen, W. (2016). The rising star in photovoltaics-perovskite solar cells: the past, present and future. Sci. China Technol. Sci. *59*, 989–1006.

Fewtrell, L., Kaufmann, R., and Prüss-Üstün, A. (2003). Lead: Assessing the Environmental Burden of Disease at National and Local Levels (World Health Organization).

Gifford, J. (2015). Dyesol Claims Perovskite Stability Breakthrough (Pv Magazine), (Last Accessed 30/10/2018). https://www.pv-magazine.com/2015/09/09/dyesol-claims-perovskite-stability-breakthrough_100021002/#axzz3lF0szmdL.

Gong, J., Darling, S.B., and You, F. (2015). Perovskite photovoltaics: life-cycle assessment of energy and environmental impacts. Energy Environ. Sci. *8*, 1953–1968.

Gottesfeld, P., and Pokhrel, A.K. (2011). Review: lead exposure in battery manufacturing and recycling in developing countries and among children in nearby communities. J. Occup. Environ. Hyg. *8*, 520–532.

Grancini, G., Roldán-Carmona, C., Zimmermann, I., Mosconi, E., Lee, X., Martineau, D., Narbey, S., Oswald, F., De Angelis, F., Graetzel, M., and Nazeeruddin, M.K. (2017). One-year stable perovskite solar cells by 2D/3D interface engineering. Nat. Commun. *8*, 15684.

Hailegnaw, B., Kirmayer, S., Edri, E., Hodes, G., and Cahen, D. (2015). Rain on methylammonium lead iodide based perovskites: possible environmental effects of perovskite solar cells. J. Phys. Chem. Lett. *6*, 1543–1547.

Hauck, M., Ligthart, T., Schaap, M., Boukris, E., and Brouwer, D. (2017). Environmental benefits of reduced electricity use exceed impacts from lead use for perovskite based tandem solar cell. Renew. Energy *111*, 906–913.

Hooper, K., Carnie, M., Charbonneau, C., and Watson, T. (2014). Near infrared radiation as a rapid heating technique for TiO 2 films on glass mounted dye-sensitized solar cells. Int. J. Photoenergy *2014*, 1–8.

Hooper, K., Smith, B., Baker, J., Greenwood, P., and Watson, T. (2015). Spray PEDOT: PSS coated perovskite with a transparent conducting electrode for low cost scalable photovoltaic devices. Mater. Res. Innov. *19*, 482–487.

Ibn-Mohammed, T., Koh, S.C.L., Reaney, I.M., Acquaye, A., Schileo, G., Mustapha, K.B., and Greenough, R. (2017). Perovskite solar cells: an integrated hybrid lifecycle assessment and review in comparison with other photovoltaic technologies. Renew. Sustain. Energy Rev. *80*, 1321–1344.

Itten, R., and Stucki, M. (2017). Highly efficient 3rd generation multi-junction solar cells using silicon heterojunction and perovskite tandem: prospective life cycle environmental impacts. Energies *10*, 841.

Jain, S.M., Phuyal, D., Davies, M.L., Li, M., Philippe, B., De Castro, C., Qiu, Z., Kim, J., Watson, T., Tsoi, W.C., et al. (2018). An effective approach of vapour assisted morphological tailoring for reducing metal defect sites in lead-free, (CH 3 NH 3) 3 Bi 2 I 9 bismuth-based perovskite solar cells for improved performance and long-term stability. Nano Energy *49*, 614–624.

Jiang, Y., Leyden, M.R., Qiu, L., Wang, S., Ono, L.K., Wu, Z., Juarez-Perez, E.J., and Qi, Y. (2018). Combination of hybrid CVD and cation exchange for upscaling Cs-substituted mixed cation perovskite solar cells with high efficiency and stability. Adv. Funct. Mater. *28*, 1703835.

Kadro, J.M., and Hagfeldt, A. (2017). The end-of-life of perovskite PV. Joule *1*, 29–46.

Kim, M., Kim, G.-H., Oh, K.S., Jo, Y., Yoon, H., Kim, K.-H., Lee, H., Kim, J.Y., and Kim, D.S. (2017). High-temperature–short-time annealing process for high-performance large-area perovskite solar cells. ACS Nano *11*, 6057–6064.

Klaassen, C. (1980). Goodman and Gilman's the pharmacological basis of therapeutics. In Goodman and Gilman's the Pharmacological Basis of Therapeutics, L.S. Goodman and A. Gilman, eds. (Mcmillan), pp. 1615–1637.

Krýsová, H., Krýsa, J., and Kavan, L. (2018). Semi-automatic spray pyrolysis deposition of thin, transparent, titania films as blocking layers for dye-sensitized and perovskite solar cells. Beilstein J. Nanotechnol. *9*, 1135–1145.

Li, C., Li, Y., Xing, Y., Zhang, Z., Zhang, X., Li, Z., Shi, Y., Ma, T., Ma, R., Wang, K., and Wei, J. (2015). Perovskite solar cell using a two-dimensional titania nanosheet thin film as the compact layer. ACS Appl. Mater. Interfaces *7*, 15117–15122.

Liu, C., Li, W., Fan, J., and Mai, Y. (2017). A brief review on the lead element substitution in perovskite solar cells. J. Energy Chem. https://doi.org/10.1016/j.jechem.2017.10.028.

Matteocci, F., Razza, S., Di Giacomo, F., Casaluci, S., Mincuzzi, G., Brown, T.M., D'Epifanio, A., Licoccia, S., and Di Carlo, A. (2014). Solid-state solar modules based on mesoscopic organometal halide perovskite: a route towards the up-scaling process. Phys. Chem. Chem. Phys. *16*, 3918.

Mei, A., Li, X., Liu, L., Ku, Z., Liu, T., Rong, Y., Xu, M., Hu, M., Chen, J., Yang, Y., et al. (2014). A hole-conductor-free, fully printable mesoscopic perovskite solar cell with high stability. Science *345*, 295–298.

Meroni, S.M.P., Mouhamad, Y., De Rossi, F., Pockett, A., Baker, J., Escalante, R., Searle, J., Carnie, M.J., Jewell, E., Oskam, G., and Watson, T.M. (2018). Homogeneous and highly controlled deposition of low viscosity inks and application on fully printable perovskite solar cells. Sci. Technol. Adv. Mater. *19*, 1–9.

Monteiro Lunardi, M., Wing Yi Ho-Baillie, A., Alvarez-Gaitan, J.P., Moore, S., and Corkish, R. (2017). A life cycle assessment of perovskite/silicon tandem solar cells. Prog. Photovolt. Res. Appl. *25*, 679–695.

Moulder, J.F., Stickle, W.F., Sobol, P.E., and Bomben, K.D. (1992). Handbook of X-ray Photoelectron Spectroscopy: A Reference Book of Standard Spectra for Identification and Interpretation of XPS Data (Physical Electronics Division, Perkin-Elmer Corporation).

Park, N.-G., Grätzel, M., Miyasaka, T., Zhu, K., and Emery, K. (2016). Towards stable and commercially available perovskite solar cells. Nat. Energy *1*, 16152.

Peleg, R. (2015). Saule Technologies secures Japanese investor. Perovskite-info. (Last Accessed 30/10/2018). https://compoundsemiconductor.net/article/97858-polish-perovskite-firm-attracts-japanese-investor.html.

Philip, B., Jewell, E., Greenwood, P., and Weirman, C. (2016). Material and process optimization screen printing carbon graphite pastes for mass production of heating elements. J. Manuf. Process *22*, 185–191.

Qiu, L., Ono, L.K., and Qi, Y. (2018). Advances and challenges to the commercialization of organic–inorganic halide perovskite solar cell technology. Mater. Today Energy *7*, 169–189.

Rajagopal, A., Yao, K., and Jen, A.K.-Y. (2018). Toward perovskite solar cell commercialization: a perspective and research roadmap based on interfacial engineering. Adv. Mater. *30*, e1800455.

Saliba, M., Correa-Baena, J.-P., Wolff, C.M., Stolterfoht, M., Phung, N., Albrecht, S., Neher, D., and Abate, A. (2018). How to make over 20% efficient perovskite solar cells in regular (n–i–p) and inverted (p–i–n) architectures. Chem. Mater. *30*, 4193–4201.

Saliba, M., Matsui, T., Domanski, K., Seo, J.-Y., Ummadisingu, A., Zakeeruddin, S.M., Correa-Baena, J.-P., Tress, W.R., Abate, A., Hagfeldt, A., and Gratzel, M. (2016). Incorporation of rubidium cations into perovskite solar cells improves photovoltaic performance. Science *354*, 206–209.

Schmidt, T.M., Larsen-Olsen, T.T., Carlé, J.E., Angmo, D., and Krebs, F.C. (2015). Upscaling of perovskite solar cells: fully ambient roll processing of flexible perovskite solar cells with printed back electrodes. Adv. Energy Mater. *5*, 1500569.

Serrano-Lujan, L., Espinosa, N., Larsen-Olsen, T.T., Abad, J., Urbina, A., and Krebs, F.C. (2015). Tin- and lead-based perovskite solar cells under

scrutiny: an environmental perspective. Adv. Energy Mater. *5*, 1501119.

Sherahilo, T. (2018). Oxford PV Sets World Record for Perovskite Solar Cell (Oxford PV).

Shin, S.S., Yeom, E.J., Yang, W.S., Hur, S., Kim, M.G., Im, J., Seo, J., Noh, J.H., and Seok, S. (2017). Colloidally prepared La-doped BaSnO 3 electrodes for efficient, photostable perovskite solar cells. Science *356*, 167–171.

Tan, H., Jain, A., Voznyy, O., Lan, X., García de Arquer, F.P., Fan, J.Z., Quintero-Bermudez, R., Yuan, M., Zhang, B., Zhao, Y., et al. (2017). Efficient and stable solution-processed planar perovskite solar cells via contact passivation. Science *355*, 722–726.

Troughton, J., Carnie, M.J., Davies, M.L., Charbonneau, C., Jewell, E.H., Worsley, D.A., and Watson, T.M. (2016). Photonic flash-annealing of lead halide perovskite solar cells in 1 ms. J. Mater. Chem. A *4*, 3471–3476.

Troughton, J., Charbonneau, C., Carnie, M.J., Davies, M.L., Worsley, D.A., and Watson, T.M. (2015). Rapid processing of perovskite solar cells in under 2.5 seconds. J. Mater. Chem. A *3*, 9123–9127.

Yang, W.S., Park, B.-W., Jung, E.H., Jeon, N.J., Kim, Y.C., Lee, D.U., Shin, S.S., Seo, J., Kim, E.K., Noh, J.H., and Seok, S.I. (2017). Iodide management in formamidinium-lead-halide–based perovskite layers for efficient solar cells. Science *356*, 1376–1379.

Yasin, A., Guo, F., and Demopoulos, G.P. (2016). Aqueous, screen-printable paste for fabrication of mesoporous composite anatase–rutile TiO 2 nanoparticle thin films for (photo)electrochemical devices. ACS Sustain. Chem. Eng. *4*, 2173–2181.

Zhang, J., Gao, X., Deng, Y., Zha, Y., Yuan, C., (2017a). Cradle-to-grave life cycle assessment of solid-state perovskite solar cells, in: The American Association of Mechanical Engineers (Ed.), Volume 4: Bio and Sustainable Manufacturing. (ASME), p. V004T05A021. https://doi.org/10.1115/MSEC2017-2970.

Zhang, J., Gao, X., Deng, Y., Zha, Y., and Yuan, C. (2017b). Comparison of life cycle environmental impacts of different perovskite solar cell systems. Sol. Energy Mater. Sol. Cells *166*, 9–17.

Zhang, H., Wang, H., Williams, S.T., Xiong, D., Zhang, W., Chueh, C.-C., Chen, W., and Jen, A.K.-Y. (2017c). SrCl 2 derived perovskite facilitating a high efficiency of 16% in hole-conductor-free fully printable mesoscopic perovskite solar cells. Adv. Mater. *29*, 1606608.

Zhang, W., Eperon, G.E., and Snaith, H.J. (2016a). Metal halide perovskites for energy applications. Nat. Energy *1*, 16048.

Zhang, W., Yang, J., Wu, X., Hu, Y., Yu, W., Wang, J., Dong, J., Li, M., Liang, S., Hu, J., and Kumar, R.V. (2016b). A critical review on secondary lead recycling technology and its prospect. Renew. Sustain. Energy Rev. *61*, 108–122.

ISCI, Volume *9*

Supplemental Information

Perovskite Photovoltaic Modules: Life Cycle Assessment of Pre-industrial Production Process

Jaume-Adrià Alberola-Borràs, Jenny A. Baker, Francesca De Rossi, Rosario Vidal, David Beynon, Katherine E.A. Hooper, Trystan M. Watson, and Iván Mora-Seró

Supplemental Information

Supplemental Figures

Ideality coefficient is defined in the Results and Discussion section of the main manuscript. In Figure S1 a wider analysis of the ideality coefficient is shown, which includes all the categories.

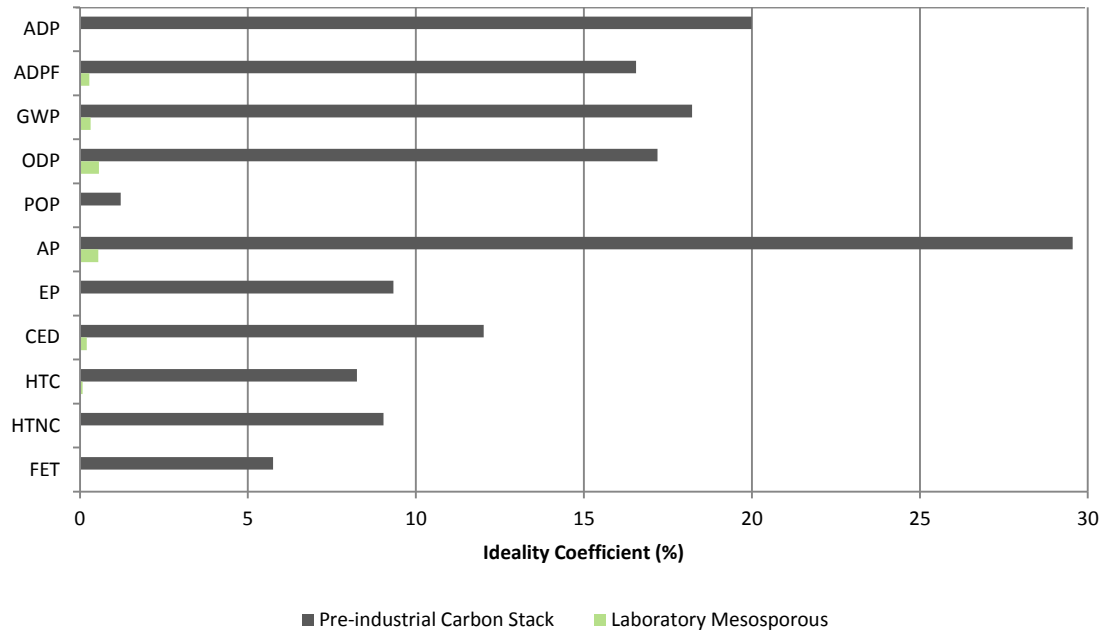

Figure S1 Ideality coefficient for the carbon stack module produced with a pre-industrial process and the PSC produced with a process in the laboratory environment. The ideality coefficient quantifies how close a given fabrication procedure from the ideal process is, in percentage; its value is the result of dividing the impact of the ideal process by the impact of the process to compare. In the vertical axis are the impact categories selected, related to Figure 4

In order to compare in great detail the carbon stack module produced at pre-industrial scale, the PSC produced at lab scale and the module produced with the ideal process, relative impacts of these three devices are displayed in Figure S2. For this analysis, the most fundamental categories are only used to ease its performance and thus its comprehension. Outcomes of this chart are obtained by dividing the impact of each device by the maximum impact within the same category and the same layer. Afterwards, the impact of each flow type pertaining to each layer is resized and aggregated to fit in the corresponding percentage of relative impact. Results are sorted by device, by category and finally by layer. Moreover, impacts of the most harmful device within the same category and the same layer have a value of 100%, whereas for the other two devices the percentage respect this device is shown. As previously discussed and according to the data reported in Figure 1 of the main manuscript, the most concerning layers of the pre-industrial module are the anode + substrate, the blocking layer and the perovskite, so these are the only layers included in the analysis.

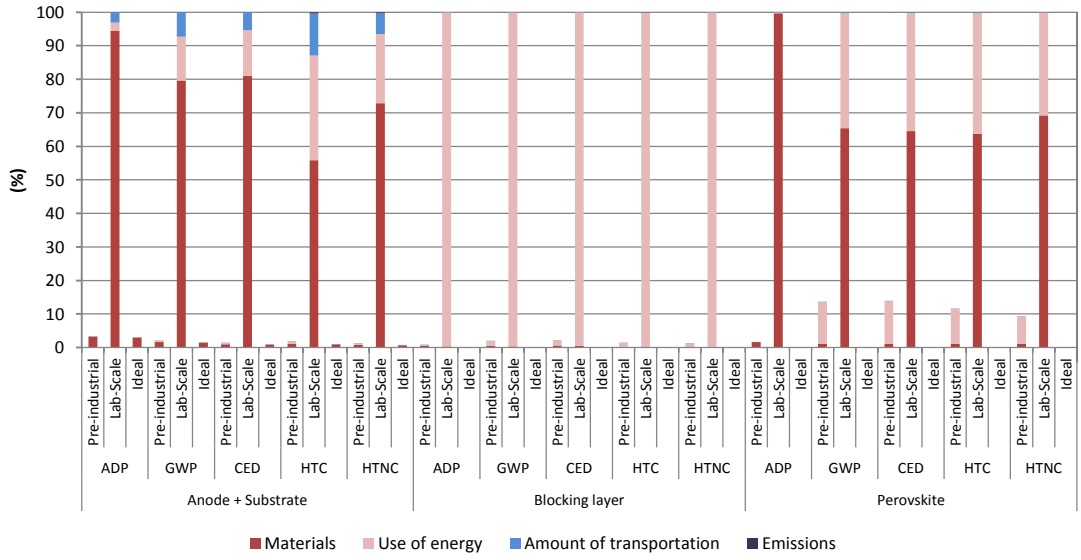

Figure S2 Relative impacts from pre-industrial module, PSC at laboratory scale and ideal process, sorted by impact categories and layers: anode + substrate, blocking and perovskite layer, related to Figure 4

Supplemental Tables

Perovskite module with a carbon stack configuration

Table S1 Inventory of the carbon stack perovskite photovoltaic module, related to Figures 1–4

Layer	Input/Output	Amount	Unit
Anode (FTO) + Substrate (glass)	Fluorine doped Tin Oxide	0.0211	g/kWh
	Glass	27.0	g/kWh
	FTO sputtering, medium voltage	$1.18 \cdot 10^{-5}$	MJ/kWh
	Laser substrate etching, medium voltage	0.0466	MJ/kWh
	Transportation burden by lorry	$7.48 \cdot 10^{-3}$	km·T/kWh
Blocking layer	Titanium di-isopropoxide bis(acetylacetonate)	0.488	g/kWh
	Isopropanol	3.63	g/kWh
	Air compression	$7.97 \cdot 10^{-6}$	m^3/kWh
	Annealing at 550 ºC for 30 min (allocated), medium voltage	0.217	MJ/kWh
	Emissions – Acetylacetone	0.796	g/kWh
	Emissions – Isopropanol	3.79	g/kWh
	Transportation burden by lorry	$1.13 \cdot 10^{-3}$	km·T/kWh
Semi conducting scaffold	Titania nanoparticles	0.0199	g/kWh
	Ethyl cellulose	0.0100	g/kWh
	2-(2-Butoxyethoxy) ethyl acetate	0.0199	g/kWh
	Terpineol	0.0586	g/kWh
	Screen printing, medium voltage	$7.72 \cdot 10^{-5}$	MJ/kWh
	Annealing at 550 ºC for 30 min (allocated), medium voltage	$8.85 \cdot 10^{-3}$	MJ/kWh
	Emissions – Titanium dioxide	$4.98 \cdot 10^{-3}$	g/kWh

	Emissions – Ethyl cellulose	$3.34 \cdot 10^{-3}$	g/kWh
	Emissions – 2-(2-Butoxyethoxy) ethyl acetate	0.0199	g/kWh
	Emissions – Terpineol	0.0586	g/kWh
	Emissions – Carbon dioxide	0.0138	g/kWh
	Emissions – Water vapour	$4.95 \cdot 10^{-3}$	g/kWh
	Transportation burden by lorry	$2.49 \cdot 10^{-5}$	km·T/kWh
	Transportation burden by freight ship	$2.08 \cdot 10^{-3}$	km·T/kWh
Insulating scaffold	Zirconia	0.0401	g/kWh
	Ethyl cellulose	0.0134	g/kWh
	Terpineol	0.0802	g/kWh
	Screen printing, medium voltage	$7.72 \cdot 10^{-5}$	MJ/kWh
	Annealing at 400 ºC for 30 min (allocated), medium voltage	0.0460	MJ/kWh
	Emissions – Zirconium dioxide	0.0100	g/kWh
	Emissions – Ethyl cellulose	$3.34 \cdot 10^{-3}$	g/kWh
	Emissions – Terpineol	0.0802	g/kWh
	Emissions – Carbon dioxide	0.0186	g/kWh
	Emissions – Water vapour	$6.65 \cdot 10^{-3}$	g/kWh
	Transportation burden by lorry	$1.63 \cdot 10^{-4}$	km·T/kWh
Cathode	Carbon	0.133	g/kWh
	Nitrocellulose	0.0222	g/kWh
	Terpineol	0.0667	g/kWh
	Screen printing, medium voltage	$7.72 \cdot 10^{-5}$	MJ/kWh
	Annealing at 400 ºC for 30 min (allocated), medium voltage	0.153	MJ/kWh
	Emissions – Carbon	0.0334	g/kWh
	Emissions – Nitrocellulose	$5.56 \cdot 10^{-3}$	g/kWh
	Emissions – Terpineol	0.0667	g/kWh
	Emissions – Carbon dioxide	0.0148	g/kWh
	Emissions – Water vapour	$3.54 \cdot 10^{-3}$	g/kWh
	Emissions – Nitrogen dioxide	$7.75 \cdot 10^{-3}$	g/kWh
	Transportation burden by lorry	$2.03 \cdot 10^{-5}$	km·T/kWh
Perovskite	Lead Iodide	0.0525	g/kWh
	Methylammonium Iodide	0.0181	g/kWh
	5-ammonium valeric acid iodide	$8.01 \cdot 10^{-4}$	g/kWh
	γ-butyrolactone	0.135	g/kWh
	Precursor solution mixture, low voltage	$5.38 \cdot 10^{-3}$	MJ/kWh
	Annealing at 50 ºC for 60 min, medium voltage	0.426	MJ/kWh
	Emissions – Butyrolactone	0.135	g/kWh
	Transportation burden by lorry	$4.86 \cdot 10^{-5}$	km·T/kWh
	Transportation burden by freight	$3.95 \cdot 10^{-4}$	km·T/kWh
Others	Screen (polyethylene terephthalate)	$1.05 \cdot 10^{-3}$	g/kWh
	Transportation burden by lorry	$3.75 \cdot 10^{-7}$	km·T/kWh

Mesoporous PSC produced in the laboratory environment

Just as it is considered for the carbon stack module, the active area is obtained by applying the fill factor, which determines the percentage of active area in respect of the overall area. This active area is then used to convert the amount of all inputs and outputs as a function of the unit of 1 kWh.

Table S2 Inventory of a mesoporous PSC produce in the laboratory environment, related to Figure 4

Layer	Input/Output	Amount	Unit
Anode (FTO) + Substrate (glass)	Fluorine doped Tin Oxide	0.562	g/kWh
	Glass	695	g/kWh
	Metallic Zinc	3.19	g/kWh
	Hydrochloric acid	3.11	g/kWh
	Deionised water	164	g/kWh
	Ethanol	123	g/kWh
	Isopropanol	123	g/kWh
	Acetone	123	g/kWh
	Soap (Hellmanex)	4.48	g/kWh
	FTO sputtering, medium voltage	0.491	MJ/kWh
	Sonication, low voltage	0.961	MJ/kWh
	Ozone chamber, medium voltage	0.184	MJ/kWh
	Emissions – Ethanol	126	g/kWh
	Emissions – Isopropanol	125	g/kWh
	Emissions – Acetone	126	g/kWh
	Emissions – Chloride	0.906	g/kWh
	Transportation burden by lorry	0.981	km·T/kWh
Electron transporting layer (ETM)	Titanium dioxide	0.138	g/kWh
	Ethanol	4.03	g/kWh
	Spin coating (2000 rpm, 1 min), low voltage	0.327	MJ/kWh
	Heating (120 ºC, 10 min), low voltage	2.09	MJ/kWh
	Annealing (450 ºC, 4h), low voltage	10.3	MJ/kWh
	Emissions – Ethanol	4.03	g/kWh
	Transportation burden by lorry	$4.11 \cdot 10^{-3}$	km·T/kWh
Scaffold	Titanium dioxide	2.62	g/kWh
	Ethanol	1.96	g/kWh
	Spin-coating (4000 rpm, 60 s), low voltage	0.675	MJ/kWh
	Heating (80 ºC, 15 min), low voltage	1.88	MJ/kWh
	Annealing (450 ºC, 4 h), low voltage	10.3	MJ/kWh
	Emissions – Ethanol	1.96.	g/kWh
	Transportation burden by lorry	$4.15 \cdot 10^{-3}$	km·T/kWh
Hole transporting	Spiro-MeOTAD	0.374	g/kWh
	Chlorobenzene	5.66	g/kWh

layer (HTM)	Spin-coating (4000 rpm, 30 s), low voltage	0.348	MJ/kWh
	Emissions – Chlorobenzene	5.66	g/kWh
	Transportation burden by lorry	$5.46 \cdot 10^{-3}$	km·T/kWh
Cathode	Gold	0.0237	g/kWh
	Thermal evaporation, medium voltage	5.85	MJ/kWh
	Transportation burden by lorry	$2.15 \cdot 10^{-5}$	km·T/kWh
Perovskite	Lead Iodide	3.28	g/kWh
	Methylammonium Iodide	1.13	g/kWh
	γ-butyrolactone	6.61	g/kWh
	Stirring (100 ºC, 10 min)	0.0818	MJ/kWh
	Stirring (70 ºC, 30 min), low voltage	0.225	MJ/kWh
	Spin-coating (500 rpm, 5 s), low voltage	0.0204	MJ/kWh
	Spin-coating (2000 rpm, 60 s), low voltage	0.327	MJ/kWh
	Heating (100 ºC, 60 min), low voltage	0.409	MJ/kWh
	Emissions – γ-butyrolactone	6.61	g/kWh
	Transportation burden by lorry	$9.99 \cdot 10^{-3}$	km·T/kWh
Others	Nitrogen gas	2004	g/kWh
	Glove box, medium voltage	10.9	MJ/kWh
	Emissions – Nitrogen gas	2004	g/kWh
	Transportation burden by lorry	0.164	km·T/kWh

Ideal process of production of carbon stack perovskite modules

Table S3 Inventory of the ideal process of production of the carbon stack perovskite module, related to Figure 4

Layer	Input/Output	Amount	Unit
Anode (FTO) + Substrate (glass)	Fluorine doped Tin Oxide	0.0190	g/kWh
	Glass	24.3	g/kWh
	FTO sputtering, medium voltage	$1.06 \cdot 10^{-5}$	MJ/kWh
	Transportation burden by lorry	$6.73 \cdot 10^{-3}$	km·T/kWh
Blocking layer	Titanium di-isopropoxide bis(acetylacetonate)	$4.26 \cdot 10^{-3}$	g/kWh
	Air compression	$7.97 \cdot 10^{-6}$	m^3/kWh
	Annealing at 550 ºC for 30 min (allocated), medium voltage	$1.89 \cdot 10^{-3}$	MJ/kWh
	Transportation burden by lorry	$1.00 \cdot 10^{-6}$	km·T/kWh
Semi conducting scaffold	Titania nanoparticles	0.0149	g/kWh
	Screen printing, medium voltage	$6.95 \cdot 10^{-5}$	MJ/kWh
	Annealing at 550 ºC for 30 min (allocated), medium voltage	$6.65 \cdot 10^{-3}$	MJ/kWh
	Transportation burden by lorry	$3.42 \cdot 10^{-6}$	km·T/kWh
	Transportation burden by freight ship	$3.12 \cdot 10^{-4}$	km·T/kWh
Insulating scaffold	Zirconia	0.0301	g/kWh
	Screen printing, medium voltage	$6.95 \cdot 10^{-5}$	MJ/kWh
	Annealing at 400 ºC for 30 min (allocated), medium voltage	$1.23 \cdot 10^{-3}$	MJ/kWh
	Transportation burden by lorry	$3.66 \cdot 10^{-5}$	km·T/kWh
Cathode	Carbon	0.120	g/kWh
	Screen printing, medium voltage	$6.95 \cdot 10^{-5}$	MJ/kWh
	Annealing at 400 ºC for 30 min (allocated), medium voltage	$4.91 \cdot 10^{-3}$	MJ/kWh
	Transportation burden by lorry	$1.09 \cdot 10^{-5}$	km·T/kWh
Perovskite	Lead Iodide	$2.96 \cdot 10^{-5}$	g/kWh
	Methylammonium Iodide	$1.02 \cdot 10^{-5}$	g/kWh
	5-ammonium valeric acid iodide	$1.56 \cdot 10^{-7}$	g/kWh
	Precursor solution mixture, low voltage	$9.76 \cdot 10^{-6}$	MJ/kWh
	Annealing at 50 ºC for 60 min, medium voltage	$4.09 \cdot 10^{-4}$	MJ/kWh
	Transportation burden by lorry	$9.34 \cdot 10^{-9}$	km·T/kWh
	Transportation burden by freight	$2.16 \cdot 10^{-7}$	km·T/kWh

Inventory of ethyl cellulose model

Table S4 Inventory for 1 kg of ethyl cellulose, related to Figures 1–4

Name	Value	Unit
Materials/fuels		
Cellulose fibre, inclusive blowing in	356.735	g
Ethanol from ethylene	101.359	g
Hydrochloric acid, from the reaction of hydrogen with chlorine	80.202	g
Chemical plant, organics	$4 \cdot 10^{-10}$	p
Electricity/heat		
Electricity, low voltage	$1.35 \cdot 10^{-6}$	kWh
Emissions to water		
Hydrogen chloride	80.202	g
Water	39.603	g

Inventory of α-terpineol model

Table S5 Inventory for 1 kg of α-terpineol, related to Figures 1–4

Name	Value	Unit
Materials/fuels		
Water, deionised	116.692	g
Dichloromethane	550.611	g
Hydrogen, liquid	25.935	g
Acetone, liquid	753.053	g
Acetylene	337.602	g
Chemical plant, organics	$4 \cdot 10^{-10}$	p
Electricity/heat		
Electricity, low voltage	0.420	kWh
Emissions to water		
Hydrogen chloride	236.366	g
Water	116.692	g
Organic chlorine compounds (unspecified)	431.03	g

Inventory of titanium di-isopropoxide bis(acetylacetonate) model

Table S6 Inventory for 1 kg of titanium di-isopropoxide bis(acetylacetonate), related to Figures 1–4

Name	Value	Unit
Materials/fuels		
Acetone, liquid, at plant	637.786	g
Titanium tetrachloride	520.724	g
Isopropanol	659.968	g
Chemical plant, organics	$4 \cdot 10^{-10}$	p
Electricity/heat		
Electricity, low voltage	$1.35 \cdot 10^{-6}$	kWh
Emissions to water		
2-Propanol	329.984	g
Methane	87.849	g
Hydrogen chloride	400.373	g

Inventory of 5-ammonium valeric acid iodide

Table S7 Inventory for 1 kg of 5-ammonium valeric acid iodide, related to Figures 1–4

Name	Value	Unit
Materials/fuels		
Formic acid	187.828	g
Butane-1,4-diol	367.49	g
Ammonia, liquid	69.541	g
Hydrogen, liquid	4.083	g
Iodine	518.18	g
Chemical plant, organics	$4 \cdot 10^{-10}$	p
Electricity/heat		
Electricity, low voltage	$1.35 \cdot 10^{-6}$	kWh
Emissions to water		
Water	146.996	g

Inventory of 2-(2-butoxyethoxy) ethyl acetate model

Table S8 Inventory for 1 kg of 2-(2-butoxyethoxy) ethyl acetate, related to Figures 1–4

Name	Value	Unit
Materials/fuels		
Acetic acid from acetaldehyde	293.992	g
Diethylene glycol	519.528	g
1-butanol, propylene hydroformylation	362.874	g
Chemical plant, organics	$4 \cdot 10^{-10}$	p
Electricity/heat		
Electricity, low voltage	$1.35 \cdot 10^{-6}$	kWh
Emissions to air		
Oxygen	78.329	g
Hydrogen	9.791	
Emissions to water		
Water	88.12	g

Inventory of nitrocellulose model

Table S9 Inventory for 1 kg of nitrocellulose, related to Figures 1–4

Name	Value	Unit
Materials/fuels		
Cellulose fibre	162.237	g
Nitric acid	378.302	g
Chemical plant, organics	$4 \cdot 10^{-10}$	p
Electricity/heat		
Electricity, low voltage	$1.35 \cdot 10^{-6}$	kWh
Emissions to water		
Water	243.183	g

Results

Table S10 Environmental impacts results for the carbon stack produced with the pre-industrial process given per kWh of electricity produced, related to Figures 1–4

	ADP (kg Sb eq)	ADPF (MJ)	GWP (kg CO_2 eq)	ODP (kg CFC-11 eq)	POP (kg C_2H_4 eq)	AP (kg SO_2 eq)	EP (kg PO_4^{3-} eq)	CED (MJ)	HTC (CTUh)	HTNC (CTUh)	FET (CTUe)
Total	$1.70\cdot10^{-6}$	2.25	0.165	$1.75\cdot10^{-8}$	$7.57\cdot10^{-4}$	$9.23\cdot10^{-4}$	$4.41\cdot10^{-4}$	3.57	$1.05\cdot10^{-8}$	$3.97\cdot10^{-8}$	1.36
Raw Materials	$1.66\cdot10^{-6}$	0.699	0.0445	$1.14\cdot10^{-8}$	$2.09\cdot10^{-5}$	$3.52\cdot10^{-4}$	$7.33\cdot10^{-5}$	0.799	$1.43\cdot10^{-9}$	$6.48\cdot10^{-9}$	0.140
Anode + Substrate	$3.71\cdot10^{-7}$	0.350	0.0294	$2.82\cdot10^{-9}$	$9.49\cdot10^{-6}$	$2.83\cdot10^{-4}$	$3.61\cdot10^{-5}$	0.388	$6.92\cdot10^{-10}$	$3.01\cdot10^{-9}$	0.0640
Fluor Tin Oxide	$3.14\cdot10^{-7}$	$4.82\cdot10^{-3}$	$3.27\cdot10^{-4}$	$2.98\cdot10^{-11}$	$3.56\cdot10^{-7}$	$8.10\cdot10^{-6}$	$1.15\cdot10^{-6}$	$6.76\cdot10^{-3}$	$4.45\cdot10^{-11}$	$1.06\cdot10^{-10}$	$2.62\cdot10^{-3}$
Solar glass, low-iron	$5.71\cdot10^{-8}$	0.345	0.0290	$2.79\cdot10^{-9}$	$9.14\cdot10^{-6}$	$2.75\cdot10^{-4}$	$3.50\cdot10^{-5}$	0.381	$6.48\cdot10^{-10}$	$2.90\cdot10^{-9}$	0.0614
Blocking layer	$1.79\cdot10^{-8}$	0.253	$8.67\cdot10^{-3}$	$4.87\cdot10^{-10}$	$9.18\cdot10^{-6}$	$3.80\cdot10^{-5}$	$1.94\cdot10^{-5}$	0.267	$2.51\cdot10^{-10}$	$1.01\cdot10^{-9}$	0.0277
Titanium diisopropoxide bis(acetylacetonate)	$4.71\cdot10^{-9}$	0.0458	$2.00\cdot10^{-3}$	$1.90\cdot10^{-10}$	$1.79\cdot10^{-6}$	$1.00\cdot10^{-5}$	$4.06\cdot10^{-6}$	0.0492	$6.91\cdot10^{-11}$	$3.21\cdot10^{-10}$	0.0116
Isopropanol	$1.32\cdot10^{-8}$	0.207	$6.67\cdot10^{-3}$	$2.96\cdot10^{-10}$	$7.39\cdot10^{-6}$	$2.80\cdot10^{-5}$	$1.53\cdot10^{-5}$	0.218	$1.81\cdot10^{-10}$	$6.86\cdot10^{-10}$	0.0161
Semi conducting scaffold	$6.44\cdot10^{-10}$	$7.19\cdot10^{-3}$	$3.90\cdot10^{-4}$	$2.19\cdot10^{-9}$	$1.19\cdot10^{-7}$	$2.03\cdot10^{-6}$	$5.97\cdot10^{-7}$	$8.62\cdot10^{-3}$	$1.90\cdot10^{-11}$	$7.62\cdot10^{-11}$	$1.76\cdot10^{-3}$
Titanium dioxide, chloride process	$1.35\cdot10^{-10}$	$1.44\cdot10^{-3}$	$8.08\cdot10^{-5}$	$1.90\cdot10^{-11}$	$1.74\cdot10^{-8}$	$4.10\cdot10^{-7}$	$2.35\cdot10^{-7}$	$1.82\cdot10^{-3}$	$4.33\cdot10^{-12}$	$2.38\cdot10^{-11}$	$7.27\cdot10^{-4}$
Ethyl cellulose	$4.25\cdot10^{-11}$	$8.20\cdot10^{-5}$	$3.30\cdot10^{-6}$	$1.56\cdot10^{-12}$	$2.28\cdot10^{-9}$	$2.23\cdot10^{-8}$	$1.01\cdot10^{-8}$	$1.11\cdot10^{-4}$	$3.54\cdot10^{-13}$	$2.46\cdot10^{-12}$	$4.68\cdot10^{-5}$
2-(2-butoxyethoxy) ethyl acetate	$1.67\cdot10^{-10}$	$1.20\cdot10^{-3}$	$4.52\cdot10^{-5}$	$2.78\cdot10^{-12}$	$2.66\cdot10^{-8}$	$1.43\cdot10^{-7}$	$5.66\cdot10^{-8}$	$1.32\cdot10^{-3}$	$1.88\cdot10^{-12}$	$9.62\cdot10^{-12}$	$2.73\cdot10^{-4}$
Terpineol	$3.00\cdot10^{-10}$	$4.47\cdot10^{-3}$	$2.60\cdot10^{-4}$	$2.16\cdot10^{-9}$	$7.29\cdot10^{-8}$	$1.45\cdot10^{-6}$	$2.96\cdot10^{-7}$	$5.37\cdot10^{-3}$	$1.24\cdot10^{-11}$	$4.04\cdot10^{-11}$	$7.14\cdot10^{-4}$
Insulating scaffold	$1.19\cdot10^{-9}$	$8.18\cdot10^{-3}$	$5.17\cdot10^{-4}$	$2.98\cdot10^{-9}$	$1.36\cdot10^{-7}$	$2.84\cdot10^{-6}$	$8.27\cdot10^{-7}$	0.0104	$2.92\cdot10^{-11}$	$1.38\cdot10^{-10}$	$2.21\cdot10^{-3}$
Zirconia	$7.18\cdot10^{-10}$	$1.95\cdot10^{-3}$	$1.56\cdot10^{-4}$	$1.08\cdot10^{-11}$	$3.32\cdot10^{-8}$	$8.21\cdot10^{-7}$	$4.08\cdot10^{-7}$	$2.85\cdot10^{-3}$	$1.17\cdot10^{-11}$	$7.89\cdot10^{-11}$	$1.17\cdot10^{-3}$
Ethyl cellulose	$5.71\cdot10^{-11}$	$1.10\cdot10^{-4}$	$4.43\cdot10^{-6}$	$2.09\cdot10^{-12}$	$3.06\cdot10^{-9}$	$2.99\cdot10^{-8}$	$1.36\cdot10^{-8}$	$1.49\cdot10^{-4}$	$4.75\cdot10^{-13}$	$3.31\cdot10^{-12}$	$6.28\cdot10^{-5}$
Terpineol	$4.11\cdot10^{-10}$	$6.12\cdot10^{-3}$	$3.57\cdot10^{-4}$	$2.96\cdot10^{-9}$	$9.98\cdot10^{-8}$	$1.99\cdot10^{-6}$	$4.05\cdot10^{-7}$	$7.36\cdot10^{-3}$	$1.70\cdot10^{-11}$	$5.53\cdot10^{-11}$	$9.78\cdot10^{-4}$
Cathode	$9.18\cdot10^{-10}$	0.0161	$6.40\cdot10^{-4}$	$2.64\cdot10^{-9}$	$1.20\cdot10^{-7}$	$2.63\cdot10^{-6}$	$4.91\cdot10^{-7}$	0.0172	$1.84\cdot10^{-11}$	$7.28\cdot10^{-11}$	$1.37\cdot10^{-3}$
Carbon	$4.68\cdot10^{-10}$	0.0108	$3.15\cdot10^{-4}$	$1.74\cdot10^{-10}$	$3.52\cdot10^{-8}$	$8.81\cdot10^{-7}$	$1.08\cdot10^{-7}$	0.0109	$3.68\cdot10^{-12}$	$2.23\cdot10^{-11}$	$4.64\cdot10^{-4}$
Nitrocellulose	$1.08\cdot10^{-10}$	$1.35\cdot10^{-4}$	$2.82\cdot10^{-5}$	$1.09\cdot10^{-12}$	$1.83\cdot10^{-9}$	$9.03\cdot10^{-8}$	$4.53\cdot10^{-8}$	$1.63\cdot10^{-4}$	$5.98\cdot10^{-13}$	$4.48\cdot10^{-12}$	$9.72\cdot10^{-5}$
Terpineol	$3.41\cdot10^{-10}$	$5.09\cdot10^{-3}$	$2.97\cdot10^{-4}$	$2.46\cdot10^{-9}$	$8.30\cdot10^{-8}$	$1.65\cdot10^{-6}$	$3.37\cdot10^{-7}$	$6.12\cdot10^{-3}$	$1.42\cdot10^{-11}$	$4.60\cdot10^{-11}$	$8.13\cdot10^{-4}$
Perovskite	$1.26\cdot10^{-6}$	0.0647	$4.90\cdot10^{-3}$	$2.95\cdot10^{-10}$	$1.87\cdot10^{-6}$	$2.36\cdot10^{-5}$	$1.58\cdot10^{-5}$	0.108	$4.22\cdot10^{-10}$	$2.17\cdot10^{-9}$	0.0427
Lead iodide	$8.90\cdot10^{-7}$	0.0438	$3.50\cdot10^{-3}$	$1.90\cdot10^{-10}$	$7.03\cdot10^{-7}$	$1.77\cdot10^{-5}$	$1.23\cdot10^{-5}$	0.0768	$3.20\cdot10^{-10}$	$1.74\cdot10^{-9}$	0.0328
Methylammonium iodide	$3.63\cdot10^{-7}$	0.0126	$9.59\cdot10^{-4}$	$5.78\cdot10^{-11}$	$1.06\cdot10^{-6}$	$4.58\cdot10^{-6}$	$2.90\cdot10^{-6}$	0.0216	$8.44\cdot10^{-11}$	$3.48\cdot10^{-10}$	$8.18\cdot10^{-3}$
5-ammonium valeric acid iodide	$1.04\cdot10^{-8}$	$6.08\cdot10^{-5}$	$3.72\cdot10^{-6}$	$5.72\cdot10^{-13}$	$9.00\cdot10^{-10}$	$1.50\cdot10^{-8}$	$4.27\cdot10^{-9}$	$6.79\cdot10^{-5}$	$1.27\cdot10^{-13}$	$7.81\cdot10^{-13}$	$1.51\cdot10^{-5}$
Gamma-butyrolactone	$7.99\cdot10^{-10}$	$8.29\cdot10^{-3}$	$4.40\cdot10^{-4}$	$4.73\cdot10^{-11}$	$1.05\cdot10^{-7}$	$1.36\cdot10^{-6}$	$5.70\cdot10^{-7}$	$9.58\cdot10^{-3}$	$1.73\cdot10^{-11}$	$8.17\cdot10^{-11}$	$1.68\cdot10^{-3}$
Others	$8.73\cdot10^{-12}$	$7.10\cdot10^{-5}$	$2.80\cdot10^{-6}$	$1.37\cdot10^{-13}$	$6.19\cdot10^{-10}$	$1.00\cdot10^{-8}$	$3.44\cdot10^{-9}$	$7.92\cdot10^{-5}$	$1.59\cdot10^{-13}$	$5.54\cdot10^{-13}$	$1.32\cdot10^{-5}$
Screen (polyethylene terephtalate)	$8.73\cdot10^{-12}$	$7.10\cdot10^{-5}$	$2.80\cdot10^{-6}$	$1.37\cdot10^{-13}$	$6.19\cdot10^{-10}$	$1.00\cdot10^{-8}$	$3.44\cdot10^{-9}$	$7.92\cdot10^{-5}$	$1.59\cdot10^{-13}$	$5.54\cdot10^{-13}$	$1.32\cdot10^{-5}$
Amount of transportation	$3.19\cdot10^{-9}$	0.0177	$1.20\cdot10^{-3}$	$1.93\cdot10^{-10}$	$2.10\cdot10^{-7}$	$6.99\cdot10^{-6}$	$1.77\cdot10^{-6}$	0.0191	$7.33\cdot10^{-11}$	$2.18\cdot10^{-10}$	$4.82\cdot10^{-3}$
Anode + Substrate transport	$2.69\cdot10^{-9}$	0.0147	$9.92\cdot10^{-4}$	$1.61\cdot10^{-10}$	$1.62\cdot10^{-7}$	$5.41\cdot10^{-6}$	$1.44\cdot10^{-6}$	0.0158	$6.11\cdot10^{-11}$	$1.82\cdot10^{-10}$	$4.03\cdot10^{-3}$
Anode + Substrate, lorry	$2.69\cdot10^{-9}$	0.0147	$9.92\cdot10^{-4}$	$1.61\cdot10^{-10}$	$1.62\cdot10^{-7}$	$5.41\cdot10^{-6}$	$1.44\cdot10^{-6}$	0.0158	$6.11\cdot10^{-11}$	$1.82\cdot10^{-10}$	$4.03\cdot10^{-3}$
Blocking layer transport	$4.06\cdot10^{-10}$	$2.21\cdot10^{-3}$	$1.50\cdot10^{-4}$	$2.42\cdot10^{-11}$	$2.44\cdot10^{-8}$	$8.16\cdot10^{-7}$	$2.18\cdot10^{-7}$	$2.38\cdot10^{-3}$	$9.22\cdot10^{-12}$	$2.75\cdot10^{-11}$	$6.08\cdot10^{-4}$

Blocking layer, lorry	$4.06 \cdot 10^{-10}$	$2.21 \cdot 10^{-3}$	$1.50 \cdot 10^{-4}$	$2.42 \cdot 10^{-11}$	$2.44 \cdot 10^{-8}$	$8.16 \cdot 10^{-7}$	$2.18 \cdot 10^{-7}$	$2.38 \cdot 10^{-3}$	$9.22 \cdot 10^{-12}$	$2.75 \cdot 10^{-11}$	$6.08 \cdot 10^{-4}$
Semi conducting scaffold transport	$1.10 \cdot 10^{-11}$	$3.45 \cdot 10^{-4}$	$2.55 \cdot 10^{-5}$	$3.07 \cdot 10^{-12}$	$1.61 \cdot 10^{-8}$	$5.08 \cdot 10^{-7}$	$5.84 \cdot 10^{-8}$	$3.84 \cdot 10^{-4}$	$9.50 \cdot 10^{-13}$	$2.44 \cdot 10^{-12}$	$5.05 \cdot 10^{-5}$
Semi conducting scaffold, lorry	$8.95 \cdot 10^{-12}$	$4.87 \cdot 10^{-5}$	$3.30 \cdot 10^{-6}$	$5.34 \cdot 10^{-13}$	$5.38 \cdot 10^{-10}$	$1.80 \cdot 10^{-8}$	$4.80 \cdot 10^{-9}$	$5.25 \cdot 10^{-5}$	$2.03 \cdot 10^{-13}$	$6.05 \cdot 10^{-13}$	$1.34 \cdot 10^{-5}$
Semi conducting scaffold, freight	$2.04 \cdot 10^{-12}$	$2.96 \cdot 10^{-4}$	$2.22 \cdot 10^{-5}$	$2.53 \cdot 10^{-12}$	$1.56 \cdot 10^{-8}$	$4.90 \cdot 10^{-7}$	$5.36 \cdot 10^{-8}$	$3.31 \cdot 10^{-4}$	$7.47 \cdot 10^{-13}$	$1.83 \cdot 10^{-12}$	$3.71 \cdot 10^{-5}$
Insulating scaffold transport	$5.85 \cdot 10^{-11}$	$3.19 \cdot 10^{-4}$	$2.16 \cdot 10^{-5}$	$3.49 \cdot 10^{-12}$	$3.52 \cdot 10^{-9}$	$1.18 \cdot 10^{-7}$	$3.14 \cdot 10^{-8}$	$3.43 \cdot 10^{-4}$	$1.33 \cdot 10^{-12}$	$3.96 \cdot 10^{-12}$	$8.76 \cdot 10^{-5}$
Insulating scaffold, lorry	$5.85 \cdot 10^{-11}$	$3.19 \cdot 10^{-4}$	$2.16 \cdot 10^{-5}$	$3.49 \cdot 10^{-12}$	$3.52 \cdot 10^{-9}$	$1.18 \cdot 10^{-7}$	$3.14 \cdot 10^{-8}$	$3.43 \cdot 10^{-4}$	$1.33 \cdot 10^{-12}$	$3.96 \cdot 10^{-12}$	$8.76 \cdot 10^{-5}$
Cathode transport	$7.29 \cdot 10^{-12}$	$3.97 \cdot 10^{-5}$	$2.69 \cdot 10^{-6}$	$4.35 \cdot 10^{-13}$	$4.38 \cdot 10^{-10}$	$1.46 \cdot 10^{-8}$	$3.91 \cdot 10^{-9}$	$4.28 \cdot 10^{-5}$	$1.65 \cdot 10^{-13}$	$4.93 \cdot 10^{-13}$	$1.09 \cdot 10^{-5}$
Cathode, lorry	$7.29 \cdot 10^{-12}$	$3.97 \cdot 10^{-5}$	$2.69 \cdot 10^{-6}$	$4.35 \cdot 10^{-13}$	$4.38 \cdot 10^{-10}$	$1.46 \cdot 10^{-8}$	$3.91 \cdot 10^{-9}$	$4.28 \cdot 10^{-5}$	$1.65 \cdot 10^{-13}$	$4.93 \cdot 10^{-13}$	$1.09 \cdot 10^{-5}$
Perovskite transport	$1.79 \cdot 10^{-11}$	$1.52 \cdot 10^{-4}$	$1.07 \cdot 10^{-5}$	$1.53 \cdot 10^{-12}$	$4.01 \cdot 10^{-9}$	$1.28 \cdot 10^{-7}$	$1.96 \cdot 10^{-8}$	$1.66 \cdot 10^{-4}$	$5.39 \cdot 10^{-13}$	$1.53 \cdot 10^{-12}$	$3.32 \cdot 10^{-5}$
Perovskite, lorry	$1.75 \cdot 10^{-11}$	$9.52 \cdot 10^{-5}$	$6.45 \cdot 10^{-6}$	$1.04 \cdot 10^{-12}$	$1.05 \cdot 10^{-9}$	$3.52 \cdot 10^{-8}$	$9.38 \cdot 10^{-9}$	$1.03 \cdot 10^{-4}$	$3.97 \cdot 10^{-13}$	$1.18 \cdot 10^{-12}$	$2.62 \cdot 10^{-5}$
Perovskite, freight	$3.88 \cdot 10^{-13}$	$5.63 \cdot 10^{-5}$	$4.21 \cdot 10^{-6}$	$4.81 \cdot 10^{-13}$	$2.96 \cdot 10^{-9}$	$9.31 \cdot 10^{-8}$	$1.02 \cdot 10^{-8}$	$6.29 \cdot 10^{-5}$	$1.42 \cdot 10^{-13}$	$3.48 \cdot 10^{-13}$	$7.04 \cdot 10^{-6}$
Others transport	$1.35 \cdot 10^{-13}$	$7.35 \cdot 10^{-7}$	$4.98 \cdot 10^{-8}$	$8.06 \cdot 10^{-15}$	$8.11 \cdot 10^{-12}$	$2.71 \cdot 10^{-10}$	$7.24 \cdot 10^{-11}$	$7.92 \cdot 10^{-7}$	$3.06 \cdot 10^{-15}$	$9.13 \cdot 10^{-15}$	$2.02 \cdot 10^{-7}$
Others, lorry	$1.35 \cdot 10^{-13}$	$7.35 \cdot 10^{-7}$	$4.98 \cdot 10^{-8}$	$8.06 \cdot 10^{-15}$	$8.11 \cdot 10^{-12}$	$2.71 \cdot 10^{-10}$	$7.24 \cdot 10^{-11}$	$7.92 \cdot 10^{-7}$	$3.06 \cdot 10^{-15}$	$9.13 \cdot 10^{-15}$	$2.02 \cdot 10^{-7}$
Use of Energy	$3.84 \cdot 10^{-8}$	1.53	0.120	$5.94 \cdot 10^{-9}$	$2.23 \cdot 10^{-5}$	$5.60 \cdot 10^{-4}$	$3.65 \cdot 10^{-4}$	2.75	$8.99 \cdot 10^{-9}$	$3.30 \cdot 10^{-8}$	0.799
Anode + Substrate	$1.92 \cdot 10^{-9}$	0.0788	$6.17 \cdot 10^{-3}$	$3.06 \cdot 10^{-10}$	$1.15 \cdot 10^{-6}$	$2.89 \cdot 10^{-5}$	$1.88 \cdot 10^{-5}$	0.142	$4.63 \cdot 10^{-10}$	$1.70 \cdot 10^{-9}$	0.0411
Blocking layer	$8.96 \cdot 10^{-9}$	0.367	0.0287	$1.42 \cdot 10^{-9}$	$5.35 \cdot 10^{-6}$	$1.34 \cdot 10^{-4}$	$8.75 \cdot 10^{-5}$	0.660	$2.15 \cdot 10^{-9}$	$7.91 \cdot 10^{-9}$	0.191
Blocking layer, medium voltage (allocated annealing)	$8.94 \cdot 10^{-9}$	0.367	0.0287	$1.42 \cdot 10^{-9}$	$5.35 \cdot 10^{-6}$	$1.34 \cdot 10^{-4}$	$8.75 \cdot 10^{-5}$	0.660	$2.15 \cdot 10^{-9}$	$7.90 \cdot 10^{-9}$	0.191
compressed air, 1000 kPa gauge	$2.07 \cdot 10^{-11}$	$1.52 \cdot 10^{-5}$	$1.23 \cdot 10^{-6}$	$7.04 \cdot 10^{-14}$	$3.60 \cdot 10^{-10}$	$7.62 \cdot 10^{-9}$	$6.02 \cdot 10^{-9}$	$2.49 \cdot 10^{-5}$	$2.95 \cdot 10^{-13}$	$1.92 \cdot 10^{-12}$	$4.18 \cdot 10^{-5}$
Semi conducting scaffold	$3.68 \cdot 10^{-10}$	0.0151	$1.18 \cdot 10^{-3}$	$5.87 \cdot 10^{-11}$	$2.20 \cdot 10^{-7}$	$5.53 \cdot 10^{-6}$	$3.60 \cdot 10^{-6}$	0.0272	$8.86 \cdot 10^{-11}$	$3.25 \cdot 10^{-10}$	$7.87 \cdot 10^{-3}$
Insulating scaffold	$1.90 \cdot 10^{-9}$	0.0780	$6.11 \cdot 10^{-3}$	$3.03 \cdot 10^{-10}$	$1.14 \cdot 10^{-6}$	$2.86 \cdot 10^{-5}$	$1.86 \cdot 10^{-5}$	0.140	$4.58 \cdot 10^{-10}$	$1.68 \cdot 10^{-9}$	0.0407
Cathode	$6.32 \cdot 10^{-9}$	0.259	0.0203	$1.01 \cdot 10^{-9}$	$3.78 \cdot 10^{-6}$	$9.49 \cdot 10^{-5}$	$6.18 \cdot 10^{-5}$	0.466	$1.52 \cdot 10^{-9}$	$5.58 \cdot 10^{-9}$	0.135
Perovskite	$1.89 \cdot 10^{-8}$	0.731	0.0572	$2.84 \cdot 10^{-9}$	$1.07 \cdot 10^{-5}$	$2.68 \cdot 10^{-4}$	$1.74 \cdot 10^{-4}$	1.31	$4.30 \cdot 10^{-9}$	$1.58 \cdot 10^{-8}$	0.383
Perovskite, low voltage	$1.37 \cdot 10^{-9}$	0.0102	$7.97 \cdot 10^{-4}$	$3.95 \cdot 10^{-11}$	$1.53 \cdot 10^{-7}$	$3.83 \cdot 10^{-6}$	$2.55 \cdot 10^{-6}$	0.0183	$7.45 \cdot 10^{-11}$	$3.01 \cdot 10^{-10}$	$7.14 \cdot 10^{-3}$
Perovskite, medium voltage	$1.76 \cdot 10^{-8}$	0.721	0.0564	$2.80 \cdot 10^{-9}$	$1.05 \cdot 10^{-5}$	$2.64 \cdot 10^{-4}$	$1.72 \cdot 10^{-4}$	1.30	$4.23 \cdot 10^{-9}$	$1.55 \cdot 10^{-8}$	0.376
Emissions	0	0	$4.72 \cdot 10^{-5}$	0	$7.13 \cdot 10^{-4}$	$3.88 \cdot 10^{-6}$	$1.01 \cdot 10^{-6}$	0	0	0	0.412
Anode + Substrate emissions	0	0	0	0	0	0	0	0	0	0	0
Blocking layer emissions	0	0	0	0	$7.13 \cdot 10^{-4}$	0	0	0	0	0	0.0646
Emissions - Acetylacetone	0	0	0	0	0	0	0	0	0	0	0.0643
Emissions - isopropanol	0	0	0	0	$7.13 \cdot 10^{-4}$	0	0	0	0	0	$3.03 \cdot 10^{-4}$
Semi conducting scaffold emissions	0	0	$1.38 \cdot 10^{-5}$	0	0	0	0	0	0	0	0.0978
Emissions - Titanium dioxide	0	0	0	0	0	0	0	0	0	0	0
Emissions - Ethyl cellulose	0	0	0	0	0	0	0	0	0	0	0
Emissions - Diethylene glycol monobutyl ether acetate	0	0	0	0	0	0	0	0	0	0	0

Emissions - Terpineol	0	0	0	0	0	0	0	0	0	0	0.0978
Emissions - Carbon dioxide	0	0	$1.38 \cdot 10^{-5}$	0	0	0	0	0	0	0	0
Emissions - Water vapour	0	0	0	0	0	0	0	0	0	0	0
Insulating scaffold emissions	0	0	$1.86 \cdot 10^{-5}$	0	0	0	0	0	0	0	0.134
Emissions - Zirconium dioxide	0	0	0	0	0	0	0	0	0	0	0
Emissions - Ethyl cellulose	0	0	0	0	0	0	0	0	0	0	0
Emissions - Terpineol	0	0	0	0	0	0	0	0	0	0	0.134
Emissions - Carbon dioxide	0	0	$1.86 \cdot 10^{-5}$	0	0	0	0	0	0	0	0
Emissions - Water vapour	0	0	0	0	0	0	0	0	0	0	0
Cathode emissions	0	0	$1.48 \cdot 10^{-5}$	0	$2.17 \cdot 10^{-7}$	$3.88 \cdot 10^{-6}$	$1.01 \cdot 10^{-6}$	0	0	0	0.112
Emissions - Carbon	0	0	0	0	0	0	0	0	0	0	0
Emissions - Nitrocellulose	0	0	0	0	0	0	0	0	0	0	$1.10 \cdot 10^{-4}$
Emissions - Terpineol	0	0	0	0	0	0	0	0	0	0	0.111
Emissions - Carbon dioxide	0	0	$1.48 \cdot 10^{-5}$	0	0	0	0	0	0	0	0
Emissions - Water vapour	0	0	0	0	0	0	0	0	0	0	0
Emissions - Nitrogen dioxide	0	0	0	0	$2.17 \cdot 10^{-7}$	$3.88 \cdot 10^{-6}$	$1.01 \cdot 10^{-6}$	0	0	0	0
Perovskite emissions	0	0	0	0	0	0	0	0	0	0	$4.04 \cdot 10^{-3}$
Emissions - butyrolactone	0	0	0	0	0	0	0	0	0	0	$4.04 \cdot 10^{-3}$

Table S11 Results of the PSC produced with the laboratory scale method given per kWh of electricity produced given per kWh of electricity produced, related to Figure 4

	ADP (kg Sb eq)	ADPF (MJ)	GWP (kg CO_2 eq)	ODP (kg CFC-11 eq)	POP (kg C_2H_4 eq)	AP (kg SO_2 eq)	EP (kg PO_4^{3-} eq)	CED (MJ)	HTC (CTUh)	HTNC (CTUh)	FET (CTUe)
Total	$9.33\cdot10^{-4}$	133	9.50	$5.35\cdot10^{-7}$	0.0906	0.0502	0.886	213	$1.04\cdot10^{-6}$	$1.24\cdot10^{-5}$	287
Raw Materials	$9.25\cdot10^{-4}$	48.6	2.89	$1.89\cdot10^{-7}$	$1.14\cdot10^{-3}$	0.0186	0.0237	62.6	$4.66\cdot10^{-7}$	$1.02\cdot10^{-5}$	234
Front contact	$1.06\cdot10^{-5}$	29.3	1.42	$9.13\cdot10^{-8}$	$7.51\cdot10^{-4}$	0.0102	$1.89\cdot10^{-3}$	31.5	$3.58\cdot10^{-8}$	$2.76\cdot10^{-7}$	3.46
Fluor Tin Oxide	$8.35\cdot10^{-6}$	0.128	$8.71\cdot10^{-3}$	$7.94\cdot10^{-10}$	$9.49\cdot10^{-6}$	$2.16\cdot10^{-4}$	$3.06\cdot10^{-5}$	0.180	$1.18\cdot10^{-9}$	$2.83\cdot10^{-9}$	0.0699
Solar glass, low-iron	$1.47\cdot10^{-6}$	8.90	0.749	$7.19\cdot10^{-8}$	$2.35\cdot10^{-4}$	$7.07\cdot10^{-3}$	$9.02\cdot10^{-4}$	9.82	$1.67\cdot10^{-8}$	$7.48\cdot10^{-8}$	1.58
Metallic Zinc	$1.57\cdot10^{-8}$	0.126	0.0107	$5.16\cdot10^{-10}$	$5.31\cdot10^{-6}$	$1.46\cdot10^{-4}$	$6.91\cdot10^{-5}$	0.177	$1.58\cdot10^{-9}$	$1.53\cdot10^{-7}$	0.744
Hydrochloric Acid	$1.96\cdot10^{-8}$	0.0341	$2.56\cdot10^{-3}$	$2.66\cdot10^{-9}$	$5.77\cdot10^{-7}$	$1.36\cdot10^{-5}$	$8.30\cdot10^{-6}$	0.0538	$2.56\cdot10^{-10}$	$2.03\cdot10^{-9}$	0.0286
Deionised Water	$7.30\cdot10^{-10}$	0.0116	$1.39\cdot10^{-3}$	$1.35\cdot10^{-10}$	$2.36\cdot10^{-7}$	$4.17\cdot10^{-6}$	$9.96\cdot10^{-7}$	0.0171	$3.54\cdot10^{-12}$	$2.85\cdot10^{-11}$	$1.04\cdot10^{-4}$
Ethanol	$2.54\cdot10^{-7}$	5.36	0.152	$4.78\cdot10^{-9}$	$1.77\cdot10^{-4}$	$4.38\cdot10^{-4}$	$2.10\cdot10^{-4}$	5.58	$4.03\cdot10^{-9}$	$1.42\cdot10^{-8}$	0.307
Isopropanol	$4.46\cdot10^{-7}$	6.99	0.225	$1.00\cdot10^{-8}$	$2.49\cdot10^{-4}$	$9.45\cdot10^{-4}$	$5.18\cdot10^{-4}$	7.35	$6.13\cdot10^{-9}$	$2.32\cdot10^{-8}$	0.544
Acetone	$5.86\cdot10^{-8}$	7.68	0.273	$7.06\cdot10^{-11}$	$6.01\cdot10^{-5}$	$1.30\cdot10^{-3}$	$1.36\cdot10^{-4}$	7.99	$5.61\cdot10^{-9}$	$3.86\cdot10^{-9}$	0.150
Soap without additives	$2.43\cdot10^{-8}$	0.0548	$-4.73\cdot10^{-3}$	$4.01\cdot10^{-10}$	$1.31\cdot10^{-5}$	$3.08\cdot10^{-5}$	$1.99\cdot10^{-5}$	0.285	$2.84\cdot10^{-10}$	$1.67\cdot10^{-9}$	0.0342
ETM	$9.28\cdot10^{-9}$	0.186	$5.56\cdot10^{-3}$	$2.88\cdot10^{-10}$	$5.94\cdot10^{-6}$	$1.72\cdot10^{-5}$	$8.51\cdot10^{-6}$	0.196	$1.62\cdot10^{-10}$	$6.32\cdot10^{-10}$	0.0151
Titanium dioxide	$9.35\cdot10^{-10}$	0.0100	$5.60\cdot10^{-4}$	$1.32\cdot10^{-10}$	$1.21\cdot10^{-7}$	$2.84\cdot10^{-6}$	$1.63\cdot10^{-6}$	0.0126	$3.00\cdot10^{-11}$	$1.65\cdot10^{-10}$	$5.04\cdot10^{-3}$
Ethanol	$8.35\cdot10^{-9}$	0.176	$5.00\cdot10^{-3}$	$1.57\cdot10^{-10}$	$5.82\cdot10^{-6}$	$1.44\cdot10^{-5}$	$6.88\cdot10^{-6}$	0.183	$1.32\cdot10^{-10}$	$4.67\cdot10^{-10}$	0.0101
Scaffold	$2.18\cdot10^{-8}$	0.276	0.0131	$2.57\cdot10^{-9}$	$5.13\cdot10^{-6}$	$6.09\cdot10^{-5}$	$3.42\cdot10^{-5}$	0.328	$6.34\cdot10^{-10}$	$3.35\cdot10^{-9}$	0.101
Titanium dioxide	$1.77\cdot10^{-8}$	0.190	0.0106	$2.50\cdot10^{-9}$	$2.29\cdot10^{-6}$	$5.39\cdot10^{-5}$	$3.09\cdot10^{-5}$	0.239	$5.70\cdot10^{-10}$	$3.12\cdot10^{-9}$	0.0957
Ethanol	$4.07\cdot10^{-9}$	0.0857	$2.43\cdot10^{-3}$	$7.64\cdot10^{-11}$	$2.84\cdot10^{-6}$	$7.00\cdot10^{-6}$	$3.35\cdot10^{-6}$	0.0892	$6.45\cdot10^{-11}$	$2.28\cdot10^{-10}$	$4.92\cdot10^{-3}$
HTM	$1.33\cdot10^{-6}$	0.339	0.0144	$5.64\cdot10^{-9}$	$2.53\cdot10^{-5}$	$6.46\cdot10^{-5}$	$6.69\cdot10^{-5}$	0.390	$8.87\cdot10^{-10}$	$4.99\cdot10^{-9}$	0.252
Spiro-MeOTAD	$1.29\cdot10^{-6}$	0.0503	$2.94\cdot10^{-3}$	$3.08\cdot10^{-10}$	$8.74\cdot10^{-7}$	$1.63\cdot10^{-5}$	$6.42\cdot10^{-6}$	0.0545	$8.93\cdot10^{-11}$	$5.28\cdot10^{-10}$	0.0120
Chlorobenzene	$3.60\cdot10^{-8}$	0.288	0.0115	$5.33\cdot10^{-9}$	$2.44\cdot10^{-5}$	$4.83\cdot10^{-5}$	$6.05\cdot10^{-5}$	0.336	$7.98\cdot10^{-10}$	$4.46\cdot10^{-9}$	0.240
Back contact	$8.34\cdot10^{-4}$	4.105	0.301	$2.92\cdot10^{-8}$	$7.96\cdot10^{-5}$	$2.75\cdot10^{-3}$	0.0178	5.02	$3.32\cdot10^{-7}$	$9.50\cdot10^{-6}$	221
Gold	$8.34\cdot10^{-4}$	4.105	0.301	$2.92\cdot10^{-8}$	$7.96\cdot10^{-5}$	$2.75\cdot10^{-3}$	0.0178	5.02	$3.32\cdot10^{-7}$	$9.50\cdot10^{-6}$	221
Perovskite	$7.82\cdot10^{-5}$	3.92	0.300	$1.77\cdot10^{-8}$	$1.15\cdot10^{-4}$	$1.45\cdot10^{-3}$	$9.78\cdot10^{-4}$	6.61	$2.61\cdot10^{-8}$	$1.34\cdot10^{-7}$	2.64
Lead iodide	$5.55\cdot10^{-5}$	2.73	0.218	$1.18\cdot10^{-8}$	$4.38\cdot10^{-5}$	$1.10\cdot10^{-3}$	$7.70\cdot10^{-4}$	4.79	$2.00\cdot10^{-8}$	$1.09\cdot10^{-7}$	2.05
Methylammonium iodide	$2.26\cdot10^{-5}$	0.783	0.0598	$3.60\cdot10^{-9}$	$6.59\cdot10^{-5}$	$2.86\cdot10^{-4}$	$1.81\cdot10^{-4}$	1.35	$5.26\cdot10^{-9}$	$2.17\cdot10^{-8}$	0.510
Gamma-butyrolactone	$3.91\cdot10^{-8}$	0.405	0.0215	$2.31\cdot10^{-9}$	$5.14\cdot10^{-6}$	$6.66\cdot10^{-5}$	$2.79\cdot10^{-5}$	0.468	$8.45\cdot10^{-10}$	$3.99\cdot10^{-9}$	0.0823
Others	$3.05\cdot10^{-7}$	10.5	0.842	$4.27\cdot10^{-8}$	$1.62\cdot10^{-4}$	$4.08\cdot10^{-3}$	$2.89\cdot10^{-3}$	18.6	$6.98\cdot10^{-8}$	$2.50\cdot10^{-7}$	6.24
Nitrogen gas for the glove box	$3.05\cdot10^{-7}$	10.5	0.842	$4.27\cdot10^{-8}$	$1.62\cdot10^{-4}$	$4.08\cdot10^{-3}$	$2.89\cdot10^{-3}$	18.6	$6.98\cdot10^{-8}$	$2.50\cdot10^{-7}$	6.24
Amount of transportation	$4.21\cdot10^{-7}$	2.29	0.155	$2.51\cdot10^{-8}$	$2.53\cdot10^{-5}$	$8.45\cdot10^{-4}$	$2.25\cdot10^{-4}$	2.47	$9.54\cdot10^{-9}$	$2.84\cdot10^{-8}$	0.630
Front contact transport	$3.53\cdot10^{-7}$	1.92	0.130	$2.11\cdot10^{-8}$	$2.12\cdot10^{-5}$	$7.10\cdot10^{-4}$	$1.89\cdot10^{-4}$	2.07	$8.01\cdot10^{-9}$	$2.39\cdot10^{-8}$	0.529
ETM transport	$1.48\cdot10^{-9}$	$8.05\cdot10^{-3}$	$5.45\cdot10^{-4}$	$8.83\cdot10^{-11}$	$8.88\cdot10^{-8}$	$2.97\cdot10^{-6}$	$7.93\cdot10^{-7}$	$8.67\cdot10^{-3}$	$3.36\cdot10^{-11}$	$1.00\cdot10^{-10}$	$2.21\cdot10^{-3}$
Scaffold transport	$1.49\cdot10^{-9}$	$8.13\cdot10^{-3}$	$5.51\cdot10^{-4}$	$8.92\cdot10^{-11}$	$8.98\cdot10^{-8}$	$3.00\cdot10^{-6}$	$8.01\cdot10^{-7}$	$8.76\cdot10^{-3}$	$3.39\cdot10^{-11}$	$1.01\cdot10^{-10}$	$2.24\cdot10^{-3}$
HTM transport	$1.97\cdot10^{-9}$	0.0107	$7.24\cdot10^{-4}$	$1.17\cdot10^{-10}$	$1.18\cdot10^{-7}$	$3.95\cdot10^{-6}$	$1.05\cdot10^{-6}$	0.0115	$4.46\cdot10^{-11}$	$1.33\cdot10^{-10}$	$2.94\cdot10^{-3}$
Back contact transport	$7.73\cdot10^{-12}$	$4.21\cdot10^{-5}$	$2.85\cdot10^{-6}$	$4.61\cdot10^{-13}$	$4.64\cdot10^{-10}$	$1.55\cdot10^{-8}$	$4.14\cdot10^{-9}$	$4.53\cdot10^{-5}$	$1.75\cdot10^{-13}$	$5.22\cdot10^{-13}$	$1.16\cdot10^{-5}$
Perovskite transport	$3.59\cdot10^{-9}$	0.0196	$1.33\cdot10^{-3}$	$2.15\cdot10^{-10}$	$2.16\cdot10^{-7}$	$7.22\cdot10^{-6}$	$1.93\cdot10^{-6}$	0.0211	$8.15\cdot10^{-11}$	$2.43\cdot10^{-10}$	$5.38\cdot10^{-3}$

Glove box transport	$5.89\cdot10^{-8}$	0.320	0.0217	$3.51\cdot10^{-9}$	$3.54\cdot10^{-6}$	$1.18\cdot10^{-4}$	$3.15\cdot10^{-5}$	0.345	$1.34\cdot10^{-9}$	$3.98\cdot10^{-9}$	0.0882
Use of Energy	$7.86\cdot10^{-6}$	82.4	6.45	$3.20\cdot10^{-7}$	$1.23\cdot10^{-3}$	0.0307	0.0203	148	$5.61\cdot10^{-7}$	$2.20\cdot10^{-6}$	52.5
Front contact electricity	$2.73\cdot10^{-7}$	2.96	0.232	$1.15\cdot10^{-8}$	$4.40\cdot10^{-5}$	$1.10\cdot10^{-3}$	$7.28\cdot10^{-4}$	5.32	$2.00\cdot10^{-8}$	$7.84\cdot10^{-8}$	1.87
FTO sputtering, medium voltage	$2.02\cdot10^{-8}$	0.830	0.0650	$3.22\cdot10^{-9}$	$1.21\cdot10^{-5}$	$3.04\cdot10^{-4}$	$1.98\cdot10^{-4}$	1.49	$4.87\cdot10^{-9}$	$1.79\cdot10^{-8}$	0.433
Sonication, low voltage	$2.45\cdot10^{-7}$	1.82	0.142	$7.06\cdot10^{-9}$	$2.74\cdot10^{-5}$	$6.85\cdot10^{-4}$	$4.56\cdot10^{-4}$	3.27	$1.33\cdot10^{-8}$	$5.38\cdot10^{-8}$	1.28
Ozone chamber, medium voltage	$7.59\cdot10^{-9}$	0.311	0.0244	$1.21\cdot10^{-9}$	$4.54\cdot10^{-6}$	$1.14\cdot10^{-4}$	$7.42\cdot10^{-5}$	0.560	$1.83\cdot10^{-9}$	$6.71\cdot10^{-9}$	0.162
ETM electricity	$3.25\cdot10^{-6}$	24.1	1.89	$9.36\cdot10^{-8}$	$3.63\cdot10^{-4}$	$9.08\cdot10^{-3}$	$6.05\cdot10^{-3}$	43.3	$1.76\cdot10^{-7}$	$7.13\cdot10^{-7}$	16.9
Spin-coating (2000 rpm, 1 min), low voltage	$8.35\cdot10^{-8}$	0.619	0.0484	$2.40\cdot10^{-9}$	$9.32\cdot10^{-6}$	$2.33\cdot10^{-4}$	$1.55\cdot10^{-4}$	1.11	$4.53\cdot10^{-9}$	$1.83\cdot10^{-8}$	0.434
Heating (120 ºC, 10 min), low voltage	$5.32\cdot10^{-7}$	3.95	0.309	$1.53\cdot10^{-8}$	$5.94\cdot10^{-5}$	$1.49\cdot10^{-3}$	$9.90\cdot10^{-4}$	7.09	$2.89\cdot10^{-8}$	$1.17\cdot10^{-7}$	2.77
Annealing (450 ºC, 45 min), low voltage	$2.64\cdot10^{-6}$	19.5	1.53	$7.59\cdot10^{-8}$	$2.94\cdot10^{-4}$	$7.36\cdot10^{-3}$	$4.90\cdot10^{-3}$	35.1	$1.43\cdot10^{-7}$	$5.78\cdot10^{-7}$	13.7
Scaffold electricity	$3.29\cdot10^{-6}$	24.4	1.907	$9.46\cdot10^{-8}$	$3.67\cdot10^{-4}$	$9.18\cdot10^{-3}$	$6.12\cdot10^{-3}$	43.8	$1.78\cdot10^{-7}$	$7.21\cdot10^{-7}$	17.1
Spin-coating (4000 rpm, 60 s)	$1.72\cdot10^{-7}$	1.28	0.100	$4.96\cdot10^{-9}$	$1.92\cdot10^{-5}$	$4.81\cdot10^{-4}$	$3.20\cdot10^{-4}$	2.29	$9.34\cdot10^{-9}$	$3.78\cdot10^{-8}$	0.895
Heating (80 ºC, 15 min)	$4.80\cdot10^{-7}$	3.56	0.279	$1.38\cdot10^{-8}$	$5.36\cdot10^{-5}$	$1.34\cdot10^{-3}$	$8.93\cdot10^{-4}$	6.39	$2.61\cdot10^{-8}$	$1.05\cdot10^{-7}$	2.50
Annealing (450 ºC, 4 h)	$2.64\cdot10^{-6}$	19.5	1.53	$7.59\cdot10^{-8}$	$2.94\cdot10^{-4}$	$7.36\cdot10^{-3}$	$4.90\cdot10^{-3}$	35.1	$1.43\cdot10^{-7}$	$5.78\cdot10^{-7}$	13.7
HTM electricity	$8.87\cdot10^{-8}$	0.658	0.0515	$2.55\cdot10^{-9}$	$9.90\cdot10^{-6}$	$2.48\cdot10^{-4}$	$1.65\cdot10^{-4}$	1.18	$4.81\cdot10^{-9}$	$1.95\cdot10^{-8}$	0.461
Spin-coating (4000 rpm, 30 s), low voltage	$8.87\cdot10^{-8}$	0.658	0.0515	$2.55\cdot10^{-9}$	$9.90\cdot10^{-6}$	$2.48\cdot10^{-4}$	$1.65\cdot10^{-4}$	1.18	$4.81\cdot10^{-9}$	$1.95\cdot10^{-8}$	0.461
Back contact electricity	$2.41\cdot10^{-7}$	9.89	0.774	$3.84\cdot10^{-8}$	$1.44\cdot10^{-4}$	$3.62\cdot10^{-3}$	$2.36\cdot10^{-3}$	17.8	$5.80\cdot10^{-8}$	$2.13\cdot10^{-7}$	5.16
Thermal evaporation, medium voltage	$2.41\cdot10^{-7}$	9.89	0.774	$3.84\cdot10^{-8}$	$1.44\cdot10^{-4}$	$3.62\cdot10^{-3}$	$2.36\cdot10^{-3}$	17.8	$5.80\cdot10^{-8}$	$2.13\cdot10^{-7}$	5.16
Perovskite electricity	$2.71\cdot10^{-7}$	2.01	0.157	$7.81\cdot10^{-9}$	$3.03\cdot10^{-5}$	$7.58\cdot10^{-4}$	$5.05\cdot10^{-4}$	3.61	$1.47\cdot10^{-8}$	$5.95\cdot10^{-8}$	1.41
Stirring (100 ºC, 10 min)	$2.09\cdot10^{-8}$	0.155	0.0121	$6.01\cdot10^{-10}$	$2.33\cdot10^{-6}$	$5.83\cdot10^{-5}$	$3.88\cdot10^{-5}$	0.278	$1.13\cdot10^{-9}$	$4.58\cdot10^{-9}$	0.109
Stirring (70 ºC, 30 min), low voltage	$5.74\cdot10^{-8}$	0.426	0.0333	$1.65\cdot10^{-9}$	$6.41\cdot10^{-6}$	$1.60\cdot10^{-4}$	$1.07\cdot10^{-4}$	0.764	$3.11\cdot10^{-9}$	$1.26\cdot10^{-8}$	0.298
Spin-coating (500 rpm, 5 s), low voltage	$5.22\cdot10^{-9}$	0.0387	$3.03\cdot10^{-3}$	$1.50\cdot10^{-10}$	$5.82\cdot10^{-7}$	$1.46\cdot10^{-5}$	$9.71\cdot10^{-6}$	0.0695	$2.83\cdot10^{-10}$	$1.14\cdot10^{-9}$	0.0271
Spin-coating (2000 rpm, 60 s), low voltage	$8.35\cdot10^{-8}$	0.619	0.0484	$2.40\cdot10^{-9}$	$9.32\cdot10^{-6}$	$2.33\cdot10^{-4}$	$1.55\cdot10^{-4}$	1.11	$4.53\cdot10^{-9}$	$1.83\cdot10^{-8}$	0.434
Heating (100 ºC, 60 min), low voltage	$1.04\cdot10^{-7}$	0.774	0.061	$3.00\cdot10^{-9}$	$1.16\cdot10^{-5}$	$2.91\cdot10^{-4}$	$1.94\cdot10^{-4}$	1.39	$5.66\cdot10^{-9}$	$2.29\cdot10^{-8}$	0.543
Glove box electricity	$4.49\cdot10^{-7}$	18.4	1.44	$7.16\cdot10^{-8}$	$2.69\cdot10^{-4}$	$6.75\cdot10^{-3}$	$4.39\cdot10^{-3}$	33.1	$1.08\cdot10^{-7}$	$3.97\cdot10^{-7}$	9.61
Globe box, medium voltage	$4.49\cdot10^{-7}$	18.4	1.44	$7.16\cdot10^{-8}$	$2.69\cdot10^{-4}$	$6.75\cdot10^{-3}$	$4.39\cdot10^{-3}$	33.1	$1.08\cdot10^{-7}$	$3.97\cdot10^{-7}$	9.61
Emissions	0	0	0	0	0.0882	0	0.842	0	$8.77\cdot10^{-10}$	$1.41\cdot10^{-9}$	0.243
Front contact emissions	0	0	0	0	0.0858	0	0	0	$2.70\cdot10^{-10}$	$7.90\cdot10^{-10}$	0.0393
Emissions - Ethanol	0	0	0	0	0.0503	0	0	0	$2.70\cdot10^{-10}$	0	0.0193
Emissions -	0	0	0	0	0.0236	0	0	0	0	0	0.0100

Isopropanol											
Emissions - Acetone	0	0	0	0	0.0119	0	0	0	0	$7.90 \cdot 10^{-10}$	0.0100
Emissions - Chloride	0	0	0	0	0	0	0	0	0	0	0
ETM emissions	0	0	0	0	$1.61 \cdot 10^{-3}$	0	0	0	$8.62 \cdot 10^{-12}$	0	$6.16 \cdot 10^{-4}$
Emissions - Ethanol	0	0	0	0	$1.61 \cdot 10^{-3}$	0	0	0	$8.62 \cdot 10^{-12}$	0	$6.16 \cdot 10^{-4}$
Scaffold emissions	0	0	0	0	$7.83 \cdot 10^{-4}$	0	0	0	$4.20 \cdot 10^{-12}$	0	$3.00 \cdot 10^{-4}$
Emissions – Ethanol	0	0	0	0	$7.83 \cdot 10^{-4}$	0	0	0	$4.20 \cdot 10^{-12}$	0	$3.00 \cdot 10^{-4}$
HTM emissions	0	0	0	0	0	0	0	0	$5.95 \cdot 10^{-10}$	$6.17 \cdot 10^{-10}$	$4.79 \cdot 10^{-3}$
Emissions – Chlorobenzene	0	0	0	0	0	0	0	0	$5.95 \cdot 10^{-10}$	$6.17 \cdot 10^{-10}$	$4.79 \cdot 10^{-3}$
Perovskite emissions	0	0	0	0	0	0	0	0	0	0	0.198
Emissions – Butyrolactone	0	0	0	0	0	0	0	0	0	0	0.198
Glove box emissions	0	0	0	0	0	0	0.842	0	0	0	0
Emissions - Nitrogen	0	0	0	0	0	0	0.842	0	0	0	0

Table S12 Results of the ideal process of production of a carbon stack perovskite module, related to Figure 4

	ADP (kg Sb eq)	ADPF (MJ)	GWP (kg CO_2 eq)	ODP (kg CFC-11 eq)	POP (kg C_2H_4 eq)	AP (kg SO_2 eq)	EP (kg PO_4^{3-} eq)	CED (MJ)	HTC (CTUh)	HTNC (CTUh)	FET (CTUe)
Total	$3.39\cdot10^{-7}$	0.372	0.0302	$3.01\cdot10^{-9}$	$9.22\cdot10^{-6}$	$2.73\cdot10^{-4}$	$4.11\cdot10^{-5}$	0.429	$8.65\cdot10^{-10}$	$3.59\cdot10^{-9}$	0.0779
Raw Materials	$3.35\cdot10^{-7}$	0.328	0.0269	$2.72\cdot10^{-9}$	$8.63\cdot10^{-6}$	$2.56\cdot10^{-4}$	$3.32\cdot10^{-5}$	0.363	$6.39\cdot10^{-10}$	$2.81\cdot10^{-9}$	0.0596
Anode + Substrate	$3.34\cdot10^{-7}$	0.315	0.0264	$2.54\cdot10^{-9}$	$8.54\cdot10^{-6}$	$2.54\cdot10^{-4}$	$3.25\cdot10^{-5}$	0.349	$6.23\cdot10^{-10}$	$2.71\cdot10^{-9}$	0.0576
Fluor Tin Oxide	$2.82\cdot10^{-7}$	$4.34\cdot10^{-3}$	$2.94\cdot10^{-4}$	$2.68\cdot10^{-11}$	$3.21\cdot10^{-7}$	$7.29\cdot10^{-6}$	$1.03\cdot10^{-6}$	$6.09\cdot10^{-3}$	$4.00\cdot10^{-11}$	$9.57\cdot10^{-11}$	$2.36\cdot10^{-3}$
Solar glass, low-iron	$5.14\cdot10^{-8}$	0.311	0.0261	$2.51\cdot10^{-9}$	$8.22\cdot10^{-6}$	$2.47\cdot10^{-4}$	$3.15\cdot10^{-5}$	0.343	$5.83\cdot10^{-10}$	$2.61\cdot10^{-9}$	0.0552
Blocking layer	$4.11\cdot10^{-11}$	$3.99\cdot10^{-4}$	$1.74\cdot10^{-5}$	$1.66\cdot10^{-12}$	$1.56\cdot10^{-8}$	$8.73\cdot10^{-8}$	$3.55\cdot10^{-8}$	$4.29\cdot10^{-4}$	$6.03\cdot10^{-13}$	$2.80\cdot10^{-12}$	$1.01\cdot10^{-4}$
Titanium diisopropoxide bis(acetylacetonate)	$4.11\cdot10^{-11}$	$3.99\cdot10^{-4}$	$1.74\cdot10^{-5}$	$1.66\cdot10^{-12}$	$1.56\cdot10^{-8}$	$8.73\cdot10^{-8}$	$3.55\cdot10^{-8}$	$4.29\cdot10^{-4}$	$6.03\cdot10^{-13}$	$2.80\cdot10^{-12}$	$1.01\cdot10^{-4}$
Semi conducting scaffold	$1.01\cdot10^{-10}$	$1.08\cdot10^{-3}$	$6.06\cdot10^{-5}$	$1.42\cdot10^{-11}$	$1.31\cdot10^{-8}$	$3.07\cdot10^{-7}$	$1.76\cdot10^{-7}$	$1.36\cdot10^{-3}$	$3.25\cdot10^{-12}$	$1.78\cdot10^{-11}$	$5.46\cdot10^{-4}$
Titanium dioxide, chloride process, at plant/RER S	$1.01\cdot10^{-10}$	$1.08\cdot10^{-3}$	$6.06\cdot10^{-5}$	$1.42\cdot10^{-11}$	$1.31\cdot10^{-8}$	$3.07\cdot10^{-7}$	$1.76\cdot10^{-7}$	$1.36\cdot10^{-3}$	$3.25\cdot10^{-12}$	$1.78\cdot10^{-11}$	$5.46\cdot10^{-4}$
Insulating scaffold	$5.38\cdot10^{-10}$	$1.47\cdot10^{-3}$	$1.17\cdot10^{-4}$	$8.07\cdot10^{-12}$	$2.49\cdot10^{-8}$	$6.15\cdot10^{-7}$	$3.06\cdot10^{-7}$	$2.14\cdot10^{-3}$	$8.78\cdot10^{-12}$	$5.92\cdot10^{-11}$	$8.78\cdot10^{-4}$
Zirconia	$5.38\cdot10^{-10}$	$1.47\cdot10^{-3}$	$1.17\cdot10^{-4}$	$8.07\cdot10^{-12}$	$2.49\cdot10^{-8}$	$6.15\cdot10^{-7}$	$3.06\cdot10^{-7}$	$2.14\cdot10^{-3}$	$8.78\cdot10^{-12}$	$5.92\cdot10^{-11}$	$8.78\cdot10^{-4}$
Cathode	$4.21\cdot10^{-10}$	$9.76\cdot10^{-3}$	$2.84\cdot10^{-4}$	$1.56\cdot10^{-10}$	$3.17\cdot10^{-8}$	$7.92\cdot10^{-7}$	$9.74\cdot10^{-8}$	$9.82\cdot10^{-3}$	$3.31\cdot10^{-12}$	$2.01\cdot10^{-11}$	$4.18\cdot10^{-4}$
Carbon	$4.21\cdot10^{-10}$	$9.76\cdot10^{-3}$	$2.84\cdot10^{-4}$	$1.56\cdot10^{-10}$	$3.17\cdot10^{-8}$	$7.92\cdot10^{-7}$	$9.74\cdot10^{-8}$	$9.82\cdot10^{-3}$	$3.31\cdot10^{-12}$	$2.01\cdot10^{-11}$	$4.18\cdot10^{-4}$
Perovskite	$7.07\cdot10^{-10}$	$3.18\cdot10^{-5}$	$2.51\cdot10^{-6}$	$1.39\cdot10^{-13}$	$9.91\cdot10^{-10}$	$1.25\cdot10^{-8}$	$8.58\cdot10^{-9}$	$5.54\cdot10^{-5}$	$2.28\cdot10^{-13}$	$1.18\cdot10^{-12}$	$2.31\cdot10^{-5}$
Lead iodide	$5.01\cdot10^{-10}$	$2.47\cdot10^{-5}$	$1.97\cdot10^{-6}$	$1.07\cdot10^{-13}$	$3.96\cdot10^{-10}$	$9.94\cdot10^{-9}$	$6.95\cdot10^{-9}$	$4.32\cdot10^{-5}$	$1.80\cdot10^{-13}$	$9.81\cdot10^{-13}$	$1.85\cdot10^{-5}$
Methylammonium iodide	$2.04\cdot10^{-10}$	$7.07\cdot10^{-6}$	$5.40\cdot10^{-7}$	$3.25\cdot10^{-14}$	$5.95\cdot10^{-10}$	$2.58\cdot10^{-9}$	$1.63\cdot10^{-9}$	$1.21\cdot10^{-5}$	$4.75\cdot10^{-14}$	$1.96\cdot10^{-13}$	$4.60\cdot10^{-6}$
5-ammonium valeric acid iodide	$2.02\cdot10^{-12}$	$1.18\cdot10^{-8}$	$7.22\cdot10^{-10}$	$1.11\cdot10^{-16}$	$1.75\cdot10^{-13}$	$2.92\cdot10^{-12}$	$8.29\cdot10^{-13}$	$1.32\cdot10^{-8}$	$2.46\cdot10^{-17}$	$1.52\cdot10^{-16}$	$2.94\cdot10^{-9}$
Amount of transportation	$3.19\cdot10^{-9}$	0.0177	$1.20\cdot10^{-3}$	$1.93\cdot10^{-10}$	$2.10\cdot10^{-7}$	$6.99\cdot10^{-6}$	$1.77\cdot10^{-6}$	0.0191	$7.33\cdot10^{-11}$	$2.18\cdot10^{-10}$	$4.82\cdot10^{-3}$
Anode + Substrate transport	$2.42\cdot10^{-9}$	0.0132	$8.93\cdot10^{-4}$	$1.45\cdot10^{-10}$	$1.46\cdot10^{-7}$	$4.87\cdot10^{-6}$	$1.30\cdot10^{-6}$	0.0142	$5.50\cdot10^{-11}$	$1.64\cdot10^{-10}$	$3.63\cdot10^{-3}$
Anode + Substrate, lorry	$2.42\cdot10^{-9}$	0.0132	$8.93\cdot10^{-4}$	$1.45\cdot10^{-10}$	$1.46\cdot10^{-7}$	$4.87\cdot10^{-6}$	$1.30\cdot10^{-6}$	0.0142	$5.50\cdot10^{-11}$	$1.64\cdot10^{-10}$	$3.63\cdot10^{-3}$
Blocking layer transport	$3.62\cdot10^{-13}$	$1.97\cdot10^{-6}$	$1.33\cdot10^{-7}$	$2.16\cdot10^{-14}$	$2.17\cdot10^{-11}$	$7.27\cdot10^{-10}$	$1.94\cdot10^{-10}$	$2.12\cdot10^{-6}$	$8.21\cdot10^{-15}$	$2.45\cdot10^{-14}$	$5.42\cdot10^{-7}$
Blocking layer, lorry	$3.62\cdot10^{-13}$	$1.97\cdot10^{-6}$	$1.33\cdot10^{-7}$	$2.16\cdot10^{-14}$	$2.17\cdot10^{-11}$	$7.27\cdot10^{-10}$	$1.94\cdot10^{-10}$	$2.12\cdot10^{-6}$	$8.21\cdot10^{-15}$	$2.45\cdot10^{-14}$	$5.42\cdot10^{-7}$
Semi conducting scaffold transport	$1.54\cdot10^{-12}$	$5.11\cdot10^{-5}$	$3.78\cdot10^{-6}$	$4.54\cdot10^{-13}$	$2.41\cdot10^{-9}$	$7.60\cdot10^{-8}$	$8.70\cdot10^{-9}$	$5.69\cdot10^{-5}$	$1.40\cdot10^{-13}$	$3.58\cdot10^{-13}$	$7.40\cdot10^{-6}$
Semi conducting scaffold, lorry	$1.23\cdot10^{-12}$	$6.70\cdot10^{-6}$	$4.54\cdot10^{-7}$	$7.35\cdot10^{-14}$	$7.39\cdot10^{-11}$	$2.47\cdot10^{-9}$	$6.60\cdot10^{-10}$	$7.22\cdot10^{-6}$	$2.79\cdot10^{-14}$	$8.32\cdot10^{-14}$	$1.84\cdot10^{-6}$
Semi conducting scaffold, freight	$3.07\cdot10^{-13}$	$4.44\cdot10^{-5}$	$3.33\cdot10^{-6}$	$3.80\cdot10^{-13}$	$2.34\cdot10^{-9}$	$7.35\cdot10^{-8}$	$8.04\cdot10^{-9}$	$4.97\cdot10^{-5}$	$1.12\cdot10^{-13}$	$2.75\cdot10^{-13}$	$5.56\cdot10^{-6}$
Insulating scaffold transport	$1.32\cdot10^{-11}$	$7.17\cdot10^{-5}$	$4.85\cdot10^{-6}$	$7.86\cdot10^{-13}$	$7.91\cdot10^{-10}$	$2.64\cdot10^{-8}$	$7.05\cdot10^{-9}$	$7.72\cdot10^{-5}$	$2.99\cdot10^{-13}$	$8.90\cdot10^{-13}$	$1.97\cdot10^{-5}$
Insulating scaffold, lorry	$1.32\cdot10^{-11}$	$7.17\cdot10^{-5}$	$4.85\cdot10^{-6}$	$7.86\cdot10^{-13}$	$7.91\cdot10^{-10}$	$2.64\cdot10^{-8}$	$7.05\cdot10^{-9}$	$7.72\cdot10^{-5}$	$2.99\cdot10^{-13}$	$8.90\cdot10^{-13}$	$1.97\cdot10^{-5}$
Cathode transport	$3.94\cdot10^{-12}$	$2.14\cdot10^{-5}$	$1.45\cdot10^{-6}$	$2.35\cdot10^{-13}$	$2.36\cdot10^{-10}$	$7.91\cdot10^{-9}$	$2.11\cdot10^{-9}$	$2.31\cdot10^{-5}$	$8.93\cdot10^{-14}$	$2.66\cdot10^{-13}$	$5.90\cdot10^{-6}$
Cathode, lorry	$3.94\cdot10^{-12}$	$2.14\cdot10^{-5}$	$1.45\cdot10^{-6}$	$2.35\cdot10^{-13}$	$2.36\cdot10^{-10}$	$7.91\cdot10^{-9}$	$2.11\cdot10^{-9}$	$2.31\cdot10^{-5}$	$8.93\cdot10^{-14}$	$2.66\cdot10^{-13}$	$5.90\cdot10^{-6}$
Perovskite transport	$3.58\cdot10^{-15}$	$4.91\cdot10^{-8}$	$3.55\cdot10^{-9}$	$4.64\cdot10^{-16}$	$1.82\cdot10^{-12}$	$5.77\cdot10^{-11}$	$7.37\cdot10^{-12}$	$5.41\cdot10^{-8}$	$1.54\cdot10^{-16}$	$4.18\cdot10^{-16}$	$8.89\cdot10^{-9}$
Perovskite, lorry	$3.36\cdot10^{-15}$	$1.83\cdot10^{-8}$	$1.24\cdot10^{-9}$	$2.01\cdot10^{-16}$	$2.02\cdot10^{-13}$	$6.76\cdot10^{-12}$	$1.80\cdot10^{-12}$	$1.97\cdot10^{-8}$	$7.63\cdot10^{-17}$	$2.27\cdot10^{-16}$	$5.04\cdot10^{-9}$
Perovskite, freight	$2.12\cdot10^{-16}$	$3.08\cdot10^{-8}$	$2.31\cdot10^{-9}$	$2.63\cdot10^{-16}$	$1.62\cdot10^{-12}$	$5.10\cdot10^{-11}$	$5.57\cdot10^{-12}$	$3.44\cdot10^{-8}$	$7.76\cdot10^{-17}$	$1.90\cdot10^{-16}$	$3.85\cdot10^{-9}$
Use of Energy	$6.54\cdot10^{-10}$	0.0259	$2.03\cdot10^{-3}$	$1.01\cdot10^{-10}$	$3.78\cdot10^{-7}$	$9.50\cdot10^{-6}$	$6.18\cdot10^{-6}$	0.0466	$1.52\cdot10^{-10}$	$5.60\cdot10^{-10}$	0.0136

Anode + Substrate	$4.37 \cdot 10^{-13}$	$1.79 \cdot 10^{-5}$	$1.40 \cdot 10^{-6}$	$6.96 \cdot 10^{-14}$	$2.61 \cdot 10^{-10}$	$6.56 \cdot 10^{-9}$	$4.27 \cdot 10^{-9}$	$3.22 \cdot 10^{-5}$	$1.05 \cdot 10^{-13}$	$3.86 \cdot 10^{-13}$	$9.34 \cdot 10^{-6}$
Blocking layer	$9.88 \cdot 10^{-11}$	$3.22 \cdot 10^{-3}$	$2.52 \cdot 10^{-4}$	$1.25 \cdot 10^{-11}$	$4.71 \cdot 10^{-8}$	$1.18 \cdot 10^{-6}$	$7.70 \cdot 10^{-7}$	$5.79 \cdot 10^{-3}$	$1.91 \cdot 10^{-11}$	$7.10 \cdot 10^{-11}$	$1.71 \cdot 10^{-3}$
Blocking layer, medium voltage (allocated annealing)	$7.81 \cdot 10^{-11}$	$3.20 \cdot 10^{-3}$	$2.51 \cdot 10^{-4}$	$1.24 \cdot 10^{-11}$	$4.67 \cdot 10^{-8}$	$1.17 \cdot 10^{-6}$	$7.64 \cdot 10^{-7}$	$5.76 \cdot 10^{-3}$	$1.88 \cdot 10^{-11}$	$6.91 \cdot 10^{-11}$	$1.67 \cdot 10^{-3}$
compressed air, 1000 kPa gauge	$2.07 \cdot 10^{-11}$	$1.52 \cdot 10^{-5}$	$1.23 \cdot 10^{-6}$	$7.04 \cdot 10^{-14}$	$3.60 \cdot 10^{-10}$	$7.62 \cdot 10^{-9}$	$6.02 \cdot 10^{-9}$	$2.49 \cdot 10^{-5}$	$2.95 \cdot 10^{-13}$	$1.92 \cdot 10^{-12}$	$4.18 \cdot 10^{-5}$
Semi conducting scaffold	$2.77 \cdot 10^{-10}$	0.0114	$8.89 \cdot 10^{-4}$	$4.41 \cdot 10^{-11}$	$1.66 \cdot 10^{-7}$	$4.16 \cdot 10^{-6}$	$2.71 \cdot 10^{-6}$	0.0204	$6.66 \cdot 10^{-11}$	$2.45 \cdot 10^{-10}$	$5.92 \cdot 10^{-3}$
Insulating scaffold	$5.36 \cdot 10^{-11}$	$2.20 \cdot 10^{-3}$	$1.72 \cdot 10^{-4}$	$8.54 \cdot 10^{-12}$	$3.20 \cdot 10^{-8}$	$8.05 \cdot 10^{-7}$	$5.24 \cdot 10^{-7}$	$3.95 \cdot 10^{-3}$	$1.29 \cdot 10^{-11}$	$4.74 \cdot 10^{-11}$	$1.15 \cdot 10^{-3}$
Cathode	$2.05 \cdot 10^{-10}$	$8.42 \cdot 10^{-3}$	$6.59 \cdot 10^{-4}$	$3.27 \cdot 10^{-11}$	$1.23 \cdot 10^{-7}$	$3.08 \cdot 10^{-6}$	$2.01 \cdot 10^{-6}$	0.0151	$4.94 \cdot 10^{-11}$	$1.81 \cdot 10^{-10}$	$4.39 \cdot 10^{-3}$
Perovskite	$1.94 \cdot 10^{-11}$	$7.11 \cdot 10^{-4}$	$5.57 \cdot 10^{-5}$	$2.76 \cdot 10^{-12}$	$1.04 \cdot 10^{-8}$	$2.61 \cdot 10^{-7}$	$1.70 \cdot 10^{-7}$	$1.28 \cdot 10^{-3}$	$4.20 \cdot 10^{-12}$	$1.55 \cdot 10^{-11}$	$3.74 \cdot 10^{-4}$
Perovskite, low voltage	$2.49 \cdot 10^{-12}$	$1.85 \cdot 10^{-5}$	$1.45 \cdot 10^{-6}$	$7.17 \cdot 10^{-14}$	$2.78 \cdot 10^{-10}$	$6.96 \cdot 10^{-9}$	$4.64 \cdot 10^{-9}$	$3.32 \cdot 10^{-5}$	$1.35 \cdot 10^{-13}$	$5.47 \cdot 10^{-13}$	$1.30 \cdot 10^{-5}$
Perovskite, medium voltage	$1.69 \cdot 10^{-11}$	$6.92 \cdot 10^{-4}$	$5.42 \cdot 10^{-5}$	$2.69 \cdot 10^{-12}$	$1.01 \cdot 10^{-8}$	$2.54 \cdot 10^{-7}$	$1.65 \cdot 10^{-7}$	$1.25 \cdot 10^{-3}$	$4.06 \cdot 10^{-12}$	$1.49 \cdot 10^{-11}$	$3.61 \cdot 10^{-4}$

Transparent methods

Goal and scope definition

In this study, environmental impacts of a pre-industrial perovskite solar module production process are evaluated to assist researchers in their task of designing this process. We talk about pre-industrial process as large area substrates are employed in addition to industrial friendly architecture, deposition and processing techniques, however they are not fully integrated in a full production line. For this purpose, a process, close to large scale production, for fabricating perovskite modules based on a mesoporous triple stack (**pre-industrial module**) is analysed through life cycle assessment. In this work, 1 kWh of energy is assumed as a functional unit and an evaluation of the environmental impacts, from cradle to gate, is performed. This kWh of electricity was simulated/modelled to be produced assuming the actual power conversion efficiency value of the pre-industrial device (11%), the average solar radiation (1.361 $kW \cdot m^{-2}$) (Gueymard, 2018) and the best-currently-reported lifetime of a carbon stack configuration (10000 h) (Grancini et al., 2017). The size of the module is assumed to be A4-sized (210 x 297 mm).

System boundary

To simulate the environmental mark of the pre-industrial module, a production process developed in a pilot plant was considered, based on the architecture with great potential for commercialisation, i.e. the printed mesoporous stack (Baker et al., 2017; De Rossi et al., 2018). Figure S3 describes the diagram of the process studied in the cradle-to-gate life cycle assessment. Therefore, this analysis accounted for the environmental impacts ranging from the extraction of raw materials to the moment in which the device production is finished. Nevertheless, inputs generating negligible impacts such as equipment assets, maintenance, lighting, environment conditioning and labour force were disregarded (Amarakoon et al., 2017; Chatzisideris et al., 2016). Equipment assets encompass screen printer, belt oven, drying oven and squeegees together with auxiliary equipment. Polyethylene terephthalate screens — without including the metallic frame— were considered consumables because they can last for just a thousand of print cycles. As deposition of all layers, including the fluorine-doped tin oxide (FTO) film, was assumed to be completed right after the production of the substrate and the anode, the cleaning process usually applied to FTO-glass substrates was omitted as it is unnecessary. Production of encapsulation and contacts of the module were also dismissed due to its primitive state of development and thus the uncertainty of their final layout.

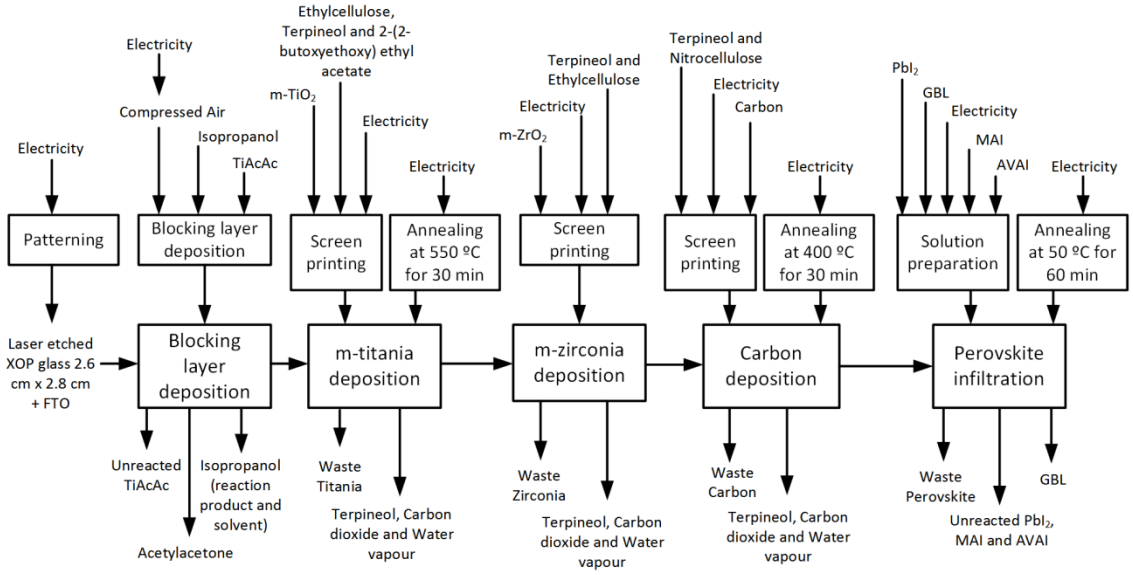

Figure S3 System boundary of the pre-industrial process of production of the carbon stack perovskite photovoltaic module, related to Figures 1–4

As shown in Figure S4, the pre-industrial module consisted of a FTO layer on top of a glass substrate, which was used as the anode and Nb:YVO_4 laser (532 nm) patterned before depositing any other layer. A layer of compact titania (c-TiO_2) was deposited by spraying a solution of titanium di-isopropoxide bis(acetylacetonate) (TiAcAc) in isopropanol (75wt%), which reacts to form the blocking layer by hydrolysis (Hanaor et al., 2012; Qin et al., 2017). An additional amount of isopropanol was added to achieve good conditions to deposit the solution. Over the blocking layer, a mesoporous layer of titania (m-TiO_2) was screen printed from a paste with α-terpineol, 2-(2-butoxyethoxy) ethyl acetate and ethylcellulose, as a semi conducting scaffold. An additional amount of α-terpineol was also added to the titania paste to reduce the final TiO_2 thickness. Both compact and m-TiO_2 were annealed in a belt electric oven at 550 ºC for 30 min. Subsequently, a paste of mesoporous zirconia (m-ZrO_2) with α-terpineol and ethylcellulose was screen printed to form the insulating scaffold. It was deposited by screen printing a paste of carbon with nitrocellulose and α-terpineol. Afterwards, m-ZrO_2 and carbon layers were annealed at 400 ºC for 30 min in the same oven as titania layers. Finally, perovskite was infiltrated to fill the pores in m-TiO_2, m-ZrO_2 and carbon layers. It was lastly annealed at 50 ºC for 1 h in a drying oven with forced convection.

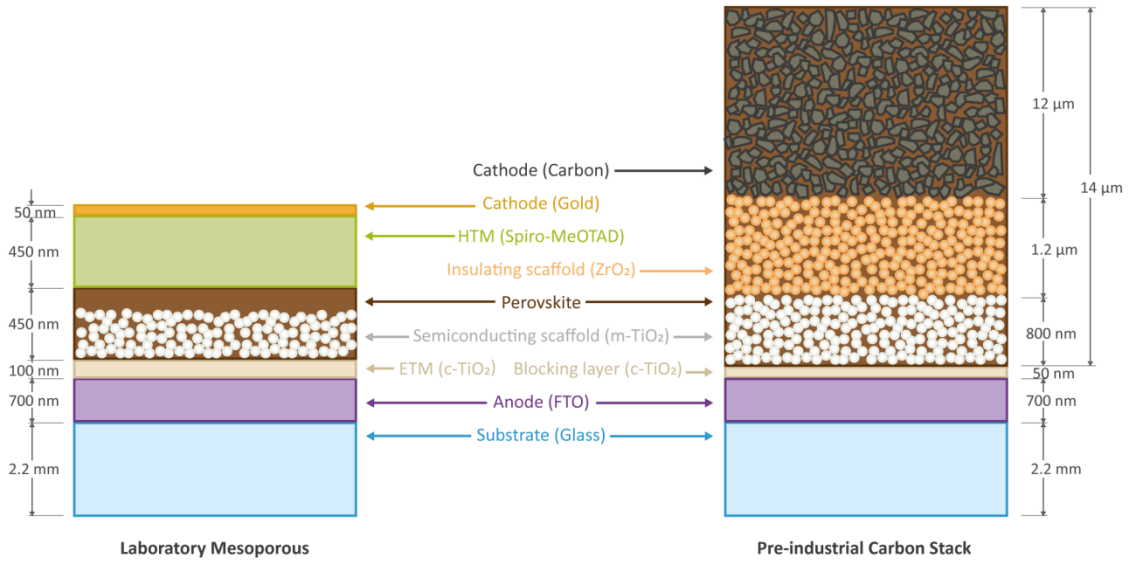

Figure S4 Dimensional cross section of the perovskite solar module produced at a pre-industrial scale (right) and the perovskite solar cell produced at a laboratory scale (left), related to Figures 1–4

Inventory

For the absorber layer of the pre-industrial module assessed in this work, a standard $MAPbI_3$ ($MA = CH_3NH_3^+$) was used. It was synthesised from 1M MAI:1M PbI_2, according to the most generalised recipe for the synthesis of perovskite (Kim et al., 2012), adding 5-ammonium valeric acid iodide (AVAI) to improve its stability (Grancini et al., 2017).

To gather data for the raw materials flow, amounts of reagents for the perovskite and c-TiO_2 syntheses, inclusive of solvents, as well as amounts of m-TiO_2, m-ZrO_2 and carbon pastes used for the production of the module were measured directly from the process. m-TiO_2, m-ZrO_2 and carbon pastes compositions were obtained from their respective producers, i.e. Greatcell Solar, Solaronix and Gwent Electronic Materials respectively. The glass and FTO film were produced by the NSG Group; in this case, as their final mass was considered, their impacts are probably underestimated.

Most of the datasets of the materials used were available at the Ecoinvent database.(Wernet et al., 2016) datasets missing in the Ecoinvent database, such as ethylcellulose, nitrocellulose (Urbanski, 1964), α-terpineol (Bellesia et al., 1979; Cori et al., 1986; Goetz and Fischer, 1976; Lu et al., 2016; Markin et al., 2016; Vani et al., 2001; Wienhöfer et al., 2013; Xiao et al., 2016), 2-(2-butoxyethoxy) ethyl acetate (Dongchu and Bing, 2016; Jung-Chung et al., 2011; Tulchinsky et al., 2010), TiAcAc (Bradley et al., 2001; Miller et al., 2001; Rahman et al., 1999; Siegel and Eggersdorfer, 2000; Weygand, 1972) and FTO (Banyamin et al., 2014; Tsang et al., 2016) together with perovskite reagents MAI (Noh et al., 2013), PbI_2 (Ahmad and Vijaya Prakash, 2012) and AVAI (Hoshi et al., 2016; Nomoto and Harada, 1985; Sato and Ota, 2016; Schaub et al., 2012), were modelled from synthesis routes encountered in the literature. The inventories of ethyl cellulose, α-terpineol, titanium di-isopropoxide bis(acetylacetonate), 5-ammonium valeric acid iodide, 2-(2-butoxyethoxy) ethyl acetate and nitrocellulose models are shown in Table S4, Table S5, Table S6, Table S7, Table S8 and Table S9, respectively. In contrast,

inventories of processes of production of FTO, MAI and PbI_2 were extracted from the literature (Alberola-Borràs et al., 2018a, 2018b).

Energy flow and energy consumption of most of the steps of the process, which are screen printing and annealing of m-TiO_2, m-ZrO_2 and Carbon pastes, annealing of perovskite and laser etching of the substrate were directly monitored from the production facilities. The energy consumption of compressed air for the screen printer was dismissed in this study as it is low in comparison to that of other steps of this process. Again, there was no information about the deposition process of the FTO layer, which was assumed to be sputtered onto the glass substrate, whose energetic consumption was obtained from other works (Tsang et al., 2016). Energy consumption to prepare the perovskite solution, by stirring and heating to 70 ºC, is obtained from a consumption value of a similar process in a previous work (Alberola-Borràs et al., 2018a). This value is recalculated to be in function of kWh (the current functional unit), as initially it was given per cm^2 of active area. It was not possible to allocate the energy consumption of the air compressor, as its use is shared by several processes, therefore, its air consumption was estimated from the amount of TiAcAc sprayed and an air to liquid ratio of 2wt% (Portoghese et al., 2008). Afterwards, the environmental impacts were directly obtained from a process dataset of compressed air in the Ecoinvent database, whose functional unit is the volume of compressed air (Wernet et al., 2016). As the blocking layer and the insulating scaffold are annealed simultaneously with the semi conducting layer and the cathode, respectively, just as Figure S3 shows, the energy consumption of each annealing process was allocated to each layer on a mass basis. Environmental impacts of the electricity consumption were established from the medium voltage and low voltage continental mix datasets for Europe (RER in Ecoinvent) (Treyer and Bauer, 2016).

Process outputs were included in the emissions flow. They were calculated stoichiometrically from the release of byproducts of the reactions of TiAcAc, which were isopropanol and acetylacetone. Likewise, combustion of ethylcellulose produced carbon dioxide and water vapour. Alongside these two gases, nitrocellulose combustion generated nitrogen oxide. Solvents of c-TiO_2 reaction, perovskite reaction and m-TiO_2, and m-ZrO_2 and carbon pastes were evaporated during annealing processes. These outputs were simulated with the coefficients for fate of emissions to the corresponding compartment available in SimaPro software (Pré Sustainability, 2016).

The amount of transportation flow was established by using the distances between each supplier and the facilities of SPECIFIC, Swansea University (UK) where the process was carried out. Transoceanic distances were considered from the closest port of each supplier to Swansea port.

Ideality analysis

Two further scenarios are used for comparison purposes: a perovskite module produced with an ideal process (**ideal module**) to estimate the ideality coefficient, based on the optimisation of the pre-industrial one, and a perovskite solar cell produced at laboratory scale (**lab-scale PSC**) to verify the extent of improvement in the pre-industrial process. From the point of view

of LCA, the comparison with the lab-scale process arises from the necessity of giving sense to the results (Baumann and Tillman, 2004). In order to obtain the electric output of both types of device, the same parameters as the pre-industrial process were assumed, except for the efficiency of the PSC in the lab process, which was 19% (Roldán-Carmona et al., 2015). The ideal scenario was estimated from the pre-industrial module, where the amounts of material used and the use of energy is ideally optimised. The environmental results of the lab-scale PSC were extracted from a previous study (Alberola-Borràs et al., 2018a), choosing a cell architecture with $MAPbI_3$ embedded into a mesoporous titania scaffold (Ball et al., 2013; Zhao et al., 2014).

The ideal process of production of perovskite solar modules was elaborated from the pre-industrial process: materials and their amounts were reduced to those strictly necessary to assemble the module and even solvents were dismissed from the system. Furthermore, energy consumption of heating steps, which were initially the most energy consuming by large, were thermodynamically estimated, considering that all the energy consumed is spent on heating the materials only and the equipment is perfectly insulated. Lastly, emissions to the environment in the ideal process were considered void, assuming a good recycling of the outputs of the process.

In the ideal process of production of perovskite modules, quantities were obtained by measuring the thicknesses of the layers in a perovskite photovoltaic module produced in a highly scalable process (Baker et al., 2017; De Rossi et al., 2018). Losses of materials during processing were excluded from this ideal scenario. Once the volume of each material was calculated by multiplying the thickness by the active module area, it was multiplied by the density to obtain the amount of each material. The transportation was re-adjusted to the reduced amount of materials for this scenario. Energy consumption of the three annealing steps and the heating and stirring of perovskite reagents was estimated by using thermodynamic equations which describe the heating process and the synthesis of the c-TiO_2 and the perovskite (Buerger et al., 2015; Degueldre et al., 2003; Ivanov et al., 2018; Knop et al., 1990; Onoda-Yamamuro et al., 1990; Saremi-Yarahmadi et al., 2013; Shinzato and Baba, 2001). No energy losses were considered during those steps. To allocate the energy of the annealing steps to each of the layers the same criteria used for the pre-industrial process is used. Since the module was considered as a single cell and divisions between cells were not necessary, laser etching was removed from the calculation. The screen printing step and consumption of air compressed for the spraying of c-TiO_2 were considered to consume the same energy as the pre-industrial process. Energy consumption of both perovskite carbon stack module and ideal process are compared in Table S13.

Table S13 Energy consumption of the carbon stack perovskite photovoltaic module produced in the pre-industrial process in comparison to the same module produced in the ideal industrial process, related to Figures 1–4

Step	Process	Carbon stack module electricity consumption (MJ/kWh)	Ideal process electricity (MJ/kWh)
Substrate production	**FTO sputtering**	0.0003	0.0003
	Laser substrate etching	1.1654	
Blocking layer deposition	**Spraying solution**	0.0002 (m^3 of air compressed)	
m-TiO_2 deposition	**Screen printing**	0.0019	0.0019
	Annealing (550 ºC, 30 min)	5.6437	0.2373
m-ZrO_2 deposition	**Screen printing**	0.0019	0.0019
Carbon deposition	**Screen printing**	0.0019	0.0019
	Annealing (400 ºC, 30 min)	4.979	0.1704
Perovskite AVA infiltration	**Solution preparation (70 ºC)**	8.944	$2.44\ 10^{-4}$
	Annealing (50 ºC, 1 hour)	10.655	0.011
Total		31.393	1.172

Inventory data of the lab-scale PSC (glass/FTO/c-TiO_2/m-TiO_2/MAPI/spiro/gold) were obtained from a previous life cycle assessment study (Alberola-Borràs et al., 2018a) and are shown in Table S2, where every parameter has been readjusted for the production of 1 kWh instead of 1 m^2. The diagram of the lab-scale PSC appears in Figure S4 compared with that of the pre-industrial module. When both pre-industrial module and lab-scale PSC were contrasted, electron and hole transporting material (ETM and HTM) and Au cathode were equated with the blocking layer, the insulating scaffold and the carbon cathode respectively.

The process of production of the lab-scale PSC consisted of a cleaning treatment of the FTO substrate, right before a compact TiO_2 layer deposition. This procedure consisted in etching a part of the FTO layer with metallic zinc and hydrochloric acid, a subsequent cleaning with 2% Hallmanex detergent and water, a sonication in isopropanol and acetone, a washing with ethanol and a final treatment with ozone plasma. Then, a mild solution of titanium isopropoxide in ethanol was deposited via spin-coating at 2000 rpm for 1 minute to obtain the the compact TiO_2 layer, after which it was heated at 120 ºC for 10 minutes and annealed at 450 ºC for 4 hours. In this step, isopropanol and ethanol vapours were emitted to the atmosphere. Onto the compact TiO_2, the perovskite layer was deposited into a 400 nm thick mesoporous TiO_2 scaffold, where TiO_2 in ethanol was spin-coated at 4000 rpm for 60 s, heated at 80 ºC for 15 minutes and annealed at 450 ºC for 4 hours. In order to deposit the perovskite into the scaffold a mixture of methylamine iodide and lead (II) iodide in γ-butyrolactone was stirred for 10 minutes at 100 ºC and for 30 minutes at 70 ºC. Then, the perovskite was spin-coated for 5 s at 500 rpm and for 60 s at 2000 rpm and finally heated at 100 ºC for 60 minutes in a drying oven. On top of it, spiro-MeOTAD in chlorobenzene was deposited by spin-coating for 30 seconds at 4000 rpm. For the back contact, gold was deposited by thermal evaporation. Nitrogen gas and electricity consumption of a glove box were also included in the inventory. The amount of electricity consumed was directly measured in the laboratory facilities and the amount of transportation was estimated from the supplier to Castelló (Spain).

Life cycle inventory assessment

Eleven impact categories were chosen and from the most developed impact models, the most representative categories were selected. Seven categories out of this group are included in the CML baseline V3.02 (de Bruijn et al., 2002; Jolliet et al., 2003). These categories encompassed: abiotic depletion, abiotic depletion (fossil fuels), global warming, ozone layer depletion, photochemical oxidation, acidification and eutrophication. Among these categories, one of the most significant to measure the environmental performance of a solar energy collector device is global warming (also known as carbon footprint), as one of the main benefits of energy stemming from such devices is the mitigation of greenhouse effect. Nonetheless, the other categories enlisted represent a broad panoply of the most concerning categories which should be taken into consideration in order to avoid environmental charge transference, from global warming category to these categories.

Energy is a fundamental aspect of perovskite modules as it is their only valuable output. Knowing the amount of energy necessary to produce them emerges as a good practice to envision how viable their production is. From the Cumulative energy demand method V1.09 (CED) (Frischknecht et al., 2005), the total cradle-to-gate energy invested in the production of the perovskite module is obtained by adding cumulative energies obtained from the different renewable and non-renewable sources provided by the method.

Pb content still remains as one of the main concerns of the possible commercialization of photovoltaics based on perovskite (Kadro and Hagfeldt, 2017). Therefore, it was necessary to include into the assessment the impact categories Human toxicity (cancer), Human toxicity (non-cancer) and Freshwater ecotoxicity from USEtox V1.04 method (Rosenbaum et al., 2008).

CML, CED and USEtox methods are incorporated within the SimaPro® 8.0.3.14 software (Pré Sustainability, 2016). In this manuscript, abbreviations listed in Table S14 are used to name the selected impact categories.

Table S14 List of impact categories, their abbreviations, units and methodologies in which they are included, related to Figures 1–4

Category	Abbreviation	Unit	Methodology
Abiotic depletion	ADP	kg Sb eq	CML baseline V3.02
Abiotic depletion, fossil fuels	ADPF	MJ	
Climate change	GWP	kg CO_2 eq	
Ozone layer depletion	ODP	kg CFC-11 eq	
Photochemical oxidation	POP	kg C_2H_4 eq	
Acidification	AP	kg SO_2 eq	
Eutrophication	EP	kg PO_4^{3-} eq	
Cumulative energy demand	CED	MJ	Cumulative energy demand V1.09
Human toxicity, cancer effects	HTC	CTUh	Usetox V1.04
Human toxicity, non-cancer effects	HTNC	CTUh	
Freshwater ecotoxicity	FET	CTUe	

Supplemental References

Ahmad, S., Vijaya Prakash, G., (2012). Fabrication of excitonic luminescent inorganic-organic hybrid nano and microcrystals, in: International Conference on Fibre Optics and Photonics. (OSA), p. MPo.40. https://doi.org/10.1364/PHOTONICS.2012.MPo.40

Alberola-Borràs, J.-A., Vidal, R., Juárez-Pérez, E.J., Mas-Marzá, E., Guerrero, A., Mora-Seró, I., (2018a). Relative impacts of methylammonium lead triiodide perovskite solar cells based on life cycle assessment. Sol. Energy Mater. Sol. Cells 179, 169–177. https://doi.org/10.1016/j.solmat.2017.11.008

Alberola-Borràs, J.-A., Vidal, R., Mora-Seró, I., (2018b). Evaluation of multiple cation/anion perovskite solar cells through life cycle assessment. Sustain. Energy Fuels 2, 1600–1609. https://doi.org/10.1039/C8SE00053K

Amarakoon, S., Vallet, C., Curran, M.A., Haldar, P., Metacarpa, D., Fobare, D., Bell, J., (2017). Life cycle assessment of photovoltaic manufacturing consortium (PVMC) copper indium gallium (di)selenide (CIGS) modules. Int. J. Life Cycle Assess. https://doi.org/10.1007/s11367-017-1345-4

Baker, J., Hooper, K., Meroni, S., Pockett, A., McGettrick, J., Wei, Z., Escalante, R., Oskam, G., Carnie, M., Watson, T., (2017). High throughput fabrication of mesoporous carbon perovskite solar cells. J. Mater. Chem. A 5, 18643–18650. https://doi.org/10.1039/C7TA05674E

Ball, J.M., Lee, M.M., Hey, A., Snaith, H.J., (2013). Low-temperature processed meso-superstructured to thin-film perovskite solar cells. Energy Environ. Sci. 6, 1739. https://doi.org/10.1039/c3ee40810h

Banyamin, Z., Kelly, P., West, G., Boardman, J., (2014). Electrical and Optical Properties of Fluorine Doped Tin Oxide Thin Films Prepared by Magnetron Sputtering. Coatings 4, 732–746. https://doi.org/10.3390/coatings4040732

Baumann, H., Tillman, A.-M., (2004). The hitch hiker's guide to LCA : an orientation in life cycle assessment methodology and application. (Studentlitteratur).

Bellesia, F., Grandi, R., Pagnoni, U.M., Trave, R., (1979). Some anomalous products from the attempted halogenation of unsaturated alcohols by the complex from dimethyl sulphide and N-halogenosuccinimide. J. Chem. Soc. Perkin Trans. 1 851. https://doi.org/10.1039/p19790000851

Bradley, D.C., Mehrotra, R.C., Rothwell, I.P., Singh, A., (2001). Alkoxo and Aryloxo Derivatives of Metals, 1st ed. (Academic Press). https://doi.org/10.1016/B978-012124140-7/50000-1

Buerger, P., Nurkowski, D., Akroyd, J., Mosbach, S., Kraft, M., (2015). First-Principles Thermochemistry for the Thermal Decomposition of Titanium Tetraisopropoxide. J. Phys. Chem. A 119, 8376–8387. https://doi.org/10.1021/acs.jpca.5b01721

Chatzisideris, M.D., Espinosa, N., Laurent, A., Krebs, F.C., (2016). Ecodesign perspectives of thin-film photovoltaic technologies: A review of life cycle assessment studies. Sol. Energy Mater. Sol. Cells 156, 2–10. https://doi.org/10.1016/j.solmat.2016.05.048

Cori, O., Chayet, L., Perez, L.M., Bunton, C.A., Hachey, D., (1986). Rearrangement of linalool, geraniol, nerol and their derivatives. J. Org. Chem. 51, 1310–1316. https://doi.org/10.1021/jo00358a028

de Bruijn, H., van Duin, R., Huijbregts, M.A.J., (2002). Handbook on Life Cycle Assessment, Operational Guide to the ISO Standards, Eco-Efficiency in Industry and Science. (Springer Netherlands). https://doi.org/10.1007/0-306-48055-7

De Rossi, F., Baker, J.A., Beynon, D., Hooper, K.E.A., Meroni, S.M.P., Williams, D., Wei, Z., Yasin, A., Charbonneau, C., Jewell, E.H., Watson, T.M., (2018). All Printable Perovskite Solar Modules with 198 cm^2 Active Area and Over 6% Efficiency. Adv. Mater. Technol. 1800156. https://doi.org/10.1002/admt.201800156

Degueldre, C., Tissot, P., Lartigue, H., Pouchon, M., (2003). Specific heat capacity and Debye temperature of zirconia and its solid solution. Thermochim. Acta 403, 267–273. https://doi.org/10.1016/S0040-6031(03)00060-1

Dongchu, W., Bing, L., (2016). Alpha, beta-unsaturated carbonyl compound production method. CN105439786A.

Frischknecht, R., Jungbluth, N., Althaus, H.-J., Doka, G., Dones, R., Heck, T., Hellweg, S., Hischier, R., Nemecek, T., Rebitzer, G., Spielmann, M., (2005). The ecoinvent Database: Overview and Methodological Framework (7 pp). Int. J. Life Cycle Assess. 10, 3–9. https://doi.org/10.1065/lca2004.10.181.1

Goetz, N., Fischer, R., (1976). Production of high molecular weight α,β-unsaturated aldehydes. US3965193 A.

Grancini, G., Roldán-Carmona, C., Zimmermann, I., Mosconi, E., Lee, X., Martineau, D., Narbey, S., Oswald, F., De Angelis, F., Graetzel, M., Nazeeruddin, M.K., (2017). One-Year stable perovskite solar cells by 2D/3D interface engineering. Nat. Commun. 8, 15684. https://doi.org/10.1038/ncomms15684

Gueymard, C.A., (2018). A reevaluation of the solar constant based on a 42-year total solar irradiance time series and a reconciliation of spaceborne observations. Sol. Energy. https://doi.org/10.1016/j.solener.2018.04.001

Hanaor, D.A.H., Chironi, I., Karatchevtseva, I., Triani, G., Sorrell, C.C., (2012). Single and mixed phase TiO 2 powders prepared by excess hydrolysis of titanium alkoxide. Adv. Appl. Ceram. 111, 149–158. https://doi.org/10.1179/1743676111Y.0000000059

Hoshi, H., Shigeeda, N., Dai, T., (2016). Improved oxidation stability of tin iodide cubic perovskite treated by 5-ammonium valeric acid iodide. Mater. Lett. 183, 391–393. https://doi.org/https://doi.org/10.1016/j.matlet.2016.07.048

Ivanov, I.L., Steparuk, A.S., Bolyachkina, M.S., Tsvetkov, D.S., Safronov, A.P., Zuev, A.Y., (2018). Thermodynamics of formation of hybrid perovskite-type methylammonium lead halides. J. Chem. Thermodyn. 116, 253–258. https://doi.org/10.1016/j.jct.2017.09.026

Jolliet, O., Margni, M., Charles, R., Humbert, S., Payet, J., Rebitzer, G., Rosenbaum, R., (2003). IMPACT 2002+: A new life cycle impact assessment methodology. Int. J. Life Cycle Assess.

8, 324–330. https://doi.org/10.1007/BF02978505

Jung-Chung, W., Ming-Yu, H., Jen-Chun, C., Jann-Chen, L., (2011). Method of Fabricating Glycol Monoalkyl Ether Acetate Using Acidic Ionic Liquid Catalyst. US20110184207A1.

Kadro, J.M., Hagfeldt, A., (2017). The End-of-Life of Perovskite PV. Joule 1, 29–46. https://doi.org/10.1016/j.joule.2017.07.013

Kim, H.-S., Lee, C.-R., Im, J.-H., Lee, K.-B., Moehl, T., Marchioro, A., Moon, S.-J., Humphry-Baker, R., Yum, J.-H., Moser, J.E., Grätzel, M., Park, N.-G., (2012). Lead Iodide Perovskite Sensitized All-Solid-State Submicron Thin Film Mesoscopic Solar Cell with Efficiency Exceeding 9%. Sci. Rep. 2, 591. https://doi.org/10.1038/srep00591

Knop, O., Wasylishen, R.E., White, M.A., Cameron, T.S., Oort, M.J.M. Van, (1990). Alkylammonium lead halides. Part 2. CH 3 NH 3 PbX 3 (X = Cl, Br, I) perovskites: cuboctahedral halide cages with isotropic cation reorientation. Can. J. Chem. 68, 412–422. https://doi.org/10.1139/v90-063

Lu, X., Zhou, W.-J., Wu, H., Liebens, A., Wu, P., (2016). Selective synthesis of ethylene oxide through liquid-phase epoxidation of ethylene with titanosilicate/H2O2 catalytic systems. Appl. Catal. A Gen. 515, 51–59. https://doi.org/10.1016/j.apcata.2016.02.001

Markin, A. V, Smirnova, N.N., Il'ichev, I.S., Dolinsky, T.I., Radbil, A.B., (2016). Thermodynamic properties of α-terpineol over the range from T → (0 to 345) K. J. Therm. Anal. Calorim. 123, 1451–1458. https://doi.org/10.1007/s10973-015-5068-0

Miller, R., Abaecherli, C., Said, A., Jackson, B., (2001). Ketenes, in: Ullmann's Encyclopedia of Industrial Chemistry. (Wiley-VCH Verlag GmbH & Co. KGaA). https://doi.org/10.1002/14356007.a15_063

Noh, J.H., Jeon, N.J., Choi, Y.C., Nazeeruddin, M.K., Grätzel, M., Seok, S. Il, (2013). Nanostructured TiO2/CH3NH3PbI3 heterojunction solar cells employing spiro-OMeTAD/Co-complex as hole-transporting material. J. Mater. Chem. A 1, 11842. https://doi.org/10.1039/c3ta12681a

Nomoto, S., Harada, K., (1985). Flame-Induced Carboxylation of Unsaturated Amines in an Aqueous Formic Acid Solution. Chem. Lett. 14, 145–148. https://doi.org/10.1246/cl.1985.145

Onoda-Yamamuro, N., Matsuo, T., Suga, H., (1990). Calorimetric and IR spectroscopic studies of phase transitions in methylammonium trihalogenoplumbates (II)†. J. Phys. Chem. Solids 51, 1383–1395. https://doi.org/10.1016/0022-3697(90)90021-7

Portoghese, F., Ferrante, L., Berruti, F., Briens, C., Chan, E., (2008). Effect of injection-nozzle operating parameters on the interaction between a gas–liquid jet and a gas–solid fluidized bed. Powder Technol. 184, 1–10. https://doi.org/10.1016/j.powtec.2007.07.029

Pré Sustainability, (2016). SimaPro.

Qin, J., Zhang, Z., Shi, W., Liu, Y., Gao, H., Mao, Y., (2017). The optimum titanium precursor of fabricating TiO2 compact layer for perovskite solar cells. Nanoscale Res. Lett. 12, 640.

https://doi.org/10.1186/s11671-017-2418-9

Rahman, M.M., Krishna, K.M., Soga, T., Jimbo, T., Umeno, M., (1999). Optical properties and X-ray photoelectron spectroscopic study of pure and Pb-doped TiO2 thin films. J. Phys. Chem. Solids 60, 201–210. https://doi.org/10.1016/S0022-3697(98)00264-9

Roldán-Carmona, C., Gratia, P., Zimmermann, I., Grancini, G., Gao, P., Graetzel, M., Nazeeruddin, M.K., (2015). High efficiency methylammonium lead triiodide perovskite solar cells: the relevance of non-stoichiometric precursors. Energy Environ. Sci. 8, 3550–3556. https://doi.org/10.1039/C5EE02555A

Rosenbaum, R.K., Bachmann, T.M., Gold, L.S., Huijbregts, M.A.J., Jolliet, O., Juraske, R., Koehler, A., Larsen, H.F., MacLeod, M., Margni, M., McKone, T.E., Payet, J., Schuhmacher, M., van de Meent, D., Hauschild, M.Z., (2008). USEtox—the UNEP-SETAC toxicity model: recommended characterisation factors for human toxicity and freshwater ecotoxicity in life cycle impact assessment. Int. J. Life Cycle Assess. 13, 532–546. https://doi.org/10.1007/s11367-008-0038-4

Saremi-Yarahmadi, S., Whittow, W., Vaidhyanathan, B., (2013). Electromagnetic simulation studies of microwave assisted heating for the processing of nanostructured iron oxide for solar driven water splitting. Appl. Surf. Sci. 275, 65–70. https://doi.org/10.1016/j.apsusc.2013.01.124

Sato, T., Ota, K., (2016). Method for producing unsaturated amine. JP2016193871 (A).

Schaub, T., Buschhaus, B., Brinks, M.K., Schelwies, M., Paciello, R., Melder, J.-P., Merger, M., (2012). Process for the preparation of primary amines by homogeneously catalyzed alcohol amination. US20120232309A1.

Shinzato, K., Baba, T., (2001). A Laser Flash Apparatus for Thermal Diffusivity and Specific Heat Capacity Measurements. J. Therm. Anal. Calorim. 64, 413–422. https://doi.org/10.1023/A:1011594609521

Siegel, H., Eggersdorfer, M., (2000). Ketones, in: Ullmann's Encyclopedia of Industrial Chemistry. (Wiley-VCH Verlag GmbH & Co. KGaA). https://doi.org/10.1002/14356007.a15_077

Treyer, K., Bauer, C., (2016). Life cycle inventories of electricity generation and power supply in version 3 of the ecoinvent database—part I: electricity generation. Int. J. Life Cycle Assess. 21, 1236–1254. https://doi.org/10.1007/s11367-013-0665-2

Tsang, M.P., Sonnemann, G.W., Bassani, D.M., (2016). A comparative human health, ecotoxicity, and product environmental assessment on the production of organic and silicon solar cells. Prog. Photovoltaics Res. Appl. 24, 645–655. https://doi.org/10.1002/pip.2704

Tulchinsky, M.L., Briggs, J.R., Rand, C.L., (2010). Polyol ethers and process for making them. US20100048940A1.

Urbanski, T., (1964). Chemistry and technology of explosives. Volume 1. (Pergamon).

Vani, P.V.S.N., Chida, A.S., Srinivasan, R., Chandrasekharam, M., Singh, A.K., (2001). SYNTHESIS OF β-IONONE. Synth. Commun. 31, 219–224. https://doi.org/10.1081/SCC-100000202

Wernet, G., Bauer, C., Steubing, B., Reinhard, J., Moreno-Ruiz, E., Weidema, B., (2016). The ecoinvent database version 3 (part I): overview and methodology. Int. J. Life Cycle Assess. 21, 1218–1230. https://doi.org/10.1007/s11367-016-1087-8

Weygand, C., (1972). Weygand/Hilgetag Preparative organic chemistry, Wiley-Interscience publication. (John Wiley & Sons, Inc.).

Wienhöfer, G., Westerhaus, F.A., Junge, K., Ludwig, R., Beller, M., (2013). A Molecularly Defined Iron-Catalyst for the Selective Hydrogenation of α,β-Unsaturated Aldehydes. Chem. - A Eur. J. 19, 7701–7707. https://doi.org/10.1002/chem.201300660

Xiao, M., Wenle, Z., Xiangru, Z., Jianping, Z., Guangyin, L., Weichao, C., Shuzhao, M., (2016). Method for continuously preparing linalool from allylic alcohol by isomerization process. CN105218312 A.

Zhao, Y., Nardes, A.M., Zhu, K., (2014). Solid-State Mesostructured Perovskite CH 3 NH 3 PbI 3 Solar Cells: Charge Transport, Recombination, and Diffusion Length. J. Phys. Chem. Lett. 5, 490–494. https://doi.org/10.1021/jz500003v